

**PREPARATION OF HYDROXYAPATITE SCAFFOLD
USING DRIED PARTICLES FOR BONE
REPLACEMENT**

Weeranuch Sukaraseranee



**A Thesis Submitted in Partial Fulfillment of the Requirements for the
Degree of Master of Engineering in Ceramic Engineering**

Suranaree University of Technology

Academic Year 2017

การเตรียมโครงร่างไฮดรอกซีแอปาทิตโดยใช้อนุภาคแกรนูไลต์ที่ได้จากการ
พ่นแห้งแบบฝอยสำหรับทดแทนกระดูก



วิทยานิพนธ์นี้เป็นส่วนหนึ่งของการศึกษาตามหลักสูตรปริญญาวิศวกรรมศาสตรบัณฑิต
สาขาวิชาวิศวกรรมเซรามิก
มหาวิทยาลัยเทคโนโลยีสุรนารี
ปีการศึกษา 2560

PREPARATION OF HYDROXYAPATITE SCAFFOLD USING DRIED PARTICLES FOR BONE REPLACEMENT

Suranaree University of Technology has approved this thesis submitted in partial fulfillment of the requirements for a Master's Degree.

Thesis Examining Committee

Dujreutai Pongkao Kashima

(Asst. Prof. Dr. Dujreutai Pongkao Kashima)

Chairperson

Sukasem W.

(Asst. Prof. Dr. Sukasem Watcharamaisakul)

Member (Thesis Advisor)

Nitinat Suppakarn

(Asst. Prof. Dr. Nitinat Suppakarn)

Member

Santi Maensiri

(Prof. Dr. Santi Maensiri)

Vice Rector for Academic Affairs
and Internationalization

Kontorn Chamniprasart

(Assoc. Prof. Flt. Lt. Dr. Kontorn Chamniprasart)

Dean of Institute of Engineering

วีรนุช ศุภระเศรษฐี : การเตรียมโครงร่างไฮดรอกซีแอปาทาइटโดยใช้อนุภาคแกรนูลที่ได้จากการพ่นแห้งแบบฝอยสำหรับทดแทนกระดูก (PREPARATION OF HYDROXYAPATITE SCAFFOLD USING DRIED PARTICLES FOR BONE REPLACEMENT)

อาจารย์ที่ปรึกษา : ผู้ช่วยศาสตราจารย์ ดร.สุขเกษม วัชรมัยสกุล, 99 หน้า

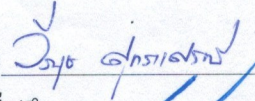
งานวิจัยนี้มีวัตถุประสงค์เพื่อศึกษาการเตรียมโครงร่างสำหรับปลูกถ่ายกระดูกเพื่อทดแทนกระดูกที่เกิดการสึกหรอ หรือเสียหายในร่างกายมนุษย์ โดยใช้ไฮดรอกซีแอปาทาइट ที่มีลักษณะเป็นอนุภาคทรงกลมที่ได้จากการเตรียมด้วยการพ่นแห้งแบบฝอย และอนุภาคทรงกลมที่ได้จากการพ่นแห้งแบบฝอยจะถูกนำมาผสมกับอนุภาคของเกล็ดขนาด 250, 325 และ 400 ไมครอน ที่อัตราส่วนแตกต่างกันระหว่างอนุภาคไฮดรอกซีแอปาทาइट กับอนุภาคเกล็ด หลังจากนั้นนำไปเผาผลาญที่ 1300 องศาเซลเซียส เพื่อให้เกล็ดย่อยออกและเกิดเป็นโครงสร้างที่มีลักษณะเป็นรูพรุน

จากการศึกษาพบว่า การเตรียมโครงร่างไฮดรอกซีแอปาทาइटโดยใช้อนุภาคทรงกลมที่ได้จากการพ่นแห้งแบบฝอยทำให้ได้โครงร่างที่มีรูพรุนหลากหลายขนาด และสามารถขึ้นรูปชิ้นงานได้ง่ายขึ้น โครงร่างเชื่อมต่อกันได้ดีและต่อเนื่อง และเมื่อผสมอนุภาคเกล็ดที่ขนาดอนุภาคต่างๆกันเข้าไปในโครงร่างหลังเผาผลาญส่งผลให้ได้รูพรุนที่มีขนาดแตกต่างกันซึ่งปริมาณรูพรุนในโครงร่างขึ้นอยู่กับขนาดของอนุภาคเกล็ด และอัตราส่วนระหว่างอนุภาคไฮดรอกซีแอปาทาइटที่เป็นอนุภาคทรงกลมและอนุภาคเกล็ด

จากการศึกษาสามารถสรุปได้ว่าปริมาณสัดส่วนระหว่างอนุภาคไฮดรอกซีแอปาทาइटและอนุภาคเกล็ด ส่งผลต่อปริมาณรูพรุนในโครงร่างสำหรับทดแทนกระดูก และการใช้ร่างไฮดรอกซีแอปาทาइटที่ได้จากการพ่นแห้งแบบฝอยทำให้ได้รูพรุนภายในโครงร่างที่หลากหลายขนาดและเหมาะสมสำหรับให้เซลล์ยึดเกาะและเจริญเติบโต

สาขาวิชา วิศวกรรมเซรามิก

ปีการศึกษา 2560

ลายมือชื่อนักศึกษา 

ลายมือชื่ออาจารย์ที่ปรึกษา 

WEERANUCH SUKARASERANEE : PREPARATION OF
HYDROXYAPATITE SCAFFOLD USING DRIED PARTICLES FOR
BONE REPLACEMENT. THESIS ADVISOR : ASST. PROF. SUKASEM
WATCHARAMAISAKUL, 99 PP.

HYDROXYAPATITE/ SPRAY DRY/ HYDROXYAPATITE SCAFFOLD/ BONE
REPLACEMENT

This thesis present study of hydroxyapatite scaffold preparation for bone replacement by used granule particle from spray dried and mixed granule particle with various sodium chloride particle include 250, 325, 400 micron at difference ratio of hydroxyapatite granule with sodium chloride particle. After that, sintering at 1300°C for sodium chloride burn out obtained to porous structure.

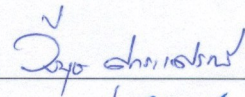
According to studies, it has been found the hydroxyapatite scaffold preparation by hydroxyapatite granule particle from spray dried obtained to various pore size, easier fabrication, and the layout is well connected and continuous connected. The sodium chloride at various particle after burn out obtained to difference size depended with sodium chloride particle size and ratio of hydroxyapatite granule particle with sodium chloride particle.

Consequently, the difference ratio of hydroxyapatite granule particle with sodium chloride particle effect to quantity of porosity in hydroxyapatite scaffold. The hydroxyapatite granule from spry dried obtained to various size of pores and optimized for cell penetrate, adhesion and proliferation.

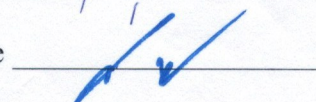
School of Ceramic Engineering

Academic Year 2017

Student's Signature



Advisor's Signature



ACKNOWLEDGMENTS

I would like to express my sincere thanks to my thesis advisor, Asst. Prof. Dr. Sukasem Watcharamaisakul and my co-advisor, Asst. Prof. Dr. Boris Golman, for their consistent supervision, comment on several thesis draft and advices throughout the process of completing this study.

I would like to express my gratitude to all teacher of the School of Ceramic Engineering for their valuable suggestion and giving me a good opportunity to study. In addition, I am grateful for the special advisor from National Metal and Materials Technology Center (MTEC), Dr. Jintamai Suwanprateep for advices.

I also would like to thanks Mrs. Pantipa Namsawangrungruang, my friends and all senior of the School of Ceramic Engineering for their help throughout the period of this research.

Finally, I most gratefully acknowledge my parents and my friends for all their support throughout the period of this research and study at Suranaree University of Technology.

Weeranuch Sukaraseranee

TABLE OF CONTENTS

	Page
ABSTRACT (THAI).....	I
ABSTRACT (ENGLISH).....	II
ACKNOWLEDGMENTS.....	III
TABLE OF CONTENTS.....	IV
LIST OF TABLES.....	VIII
LIST OF FIGURES.....	XI
CHAPTER	
I INTRODUCTION.....	1
1.1 Research objective.....	5
1.2 Scope and limitation of thesis.....	5
1.3 Expected results.....	6
II LITERATURE REVIEW.....	7
2.1 Materials.....	7
2.1.1 Hydroxyapatite ($\text{Ca}_{10}(\text{PO}_4)_6(\text{OH})_2$).....	7
2.1.2 Polyvinylpyrrolidone (PVP).....	14
2.2 Bone replacement scaffolds.....	17
2.3 Scaffold materials.....	18
2.4 Scaffold fabrication.....	21

TABLE OF CONTENTS (Continued)

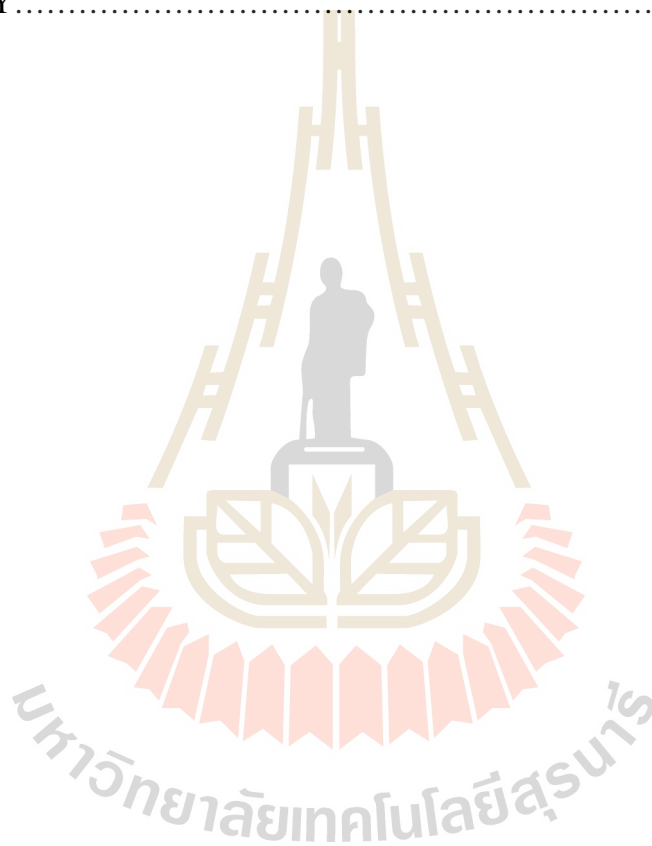
	Page
2.5 Multiscale porous scaffold.....	22
2.6 Hydroxyapatite granules by spray drying.....	22
III EXPERIMENTAL PROCEDURE.....	25
3.1 Sample preparation and analytical equipment.....	25
3.2 Materials.....	32
3.2.1 Hydroxyapatite Powder.....	33
3.2.2 Polyvinylpyrrolidone (PVP).....	33
3.2.3 Propan-2-ol (C ₃ H ₈ O).....	33
3.2.4 Maltodextrin.....	33
3.3 Characterization of raw material (Hydroxyapatite powder, sodium chloride particles)	34
3.4 Preparation of hydroxyapatite slurry for spray drying.....	34
3.5 Preparation of hydroxyapatite granules by spray drying.....	34
3.6 Characterization of spray-dried granules.....	37
3.7 Preparation of the scaffold samples.....	38
3.8 Characterization of formed samples before sintering	38
3.9 Sintering.....	38
3.10 Characterization of scaffold sample after sintering.....	39

TABLE OF CONTENTS (Continued)

		Page
IV	RESULT AND DISCUSSION.....	42
4.1	Hydroxyapatite raw material.....	42
4.1.1	Phase composition of hydroxyapatite raw material.....	42
4.2	Effect of Process Parameters on Characteristics of Spray-dried Hydroxyapatite Granules.....	43
4.2.2	Morphology of hydroxyapatite granules at difference parameters.....	43
4.2.2	Particle size distribution of hydroxyapatite granules at difference parameters.....	43
4.2.3	Flow ability of hydroxyapatite granules at difference parameters.....	43
4.3	Characteristics of drying and sintering Hydroxyapatite scaffolds at various ratio and different size of Sodium chloride... 60	60
4.3.1	Microstructure of hydroxyapatite scaffolds at various parameters before sintering.....	60
4.3.2	Microstructure sintered of hydroxyapatite.....	64
4.3.3	Characterization element composition of hydroxyapatite scaffolds.....	78
4.3.4	True porosity and bulk density of hydroxyapatite scaffold.....	79

TABLE OF CONTENTS (Continued)

	Page
V CONCLUSIONS.....	81
REFERENCE.....	84
BIOGRAPHY.....	99



LIST OF TABLES

Table	Page
2.1 Pore size distribution for an ideal scaffold in bone tissue engineering applications (Tripathi et al., 2012).....	19
3.1 Sample preparation and analytical equipment.....	25
3.2 Parameter of spray flow rate setting for control size of the final product.....	29
3.3 Materials used in experiments.....	32
3.4 Experimental spray drying conditions.....	37
4.1 Particle size distribution of hydroxyapatite granules prepared at different drying parameters.....	57
4.2 Bulk and tap densities of hydroxyapatite granules.....	58
4.3 Classification of hydroxyapatite granule flowability based on Compressibility index and Hausner ratio.....	59
4.4 Powder flowability and corresponding compressibility index and Hausner ratio.....	60
4.5 Element ratio of hydroxyapatite scaffold after sintering at 1300°C by using Energy-dispersive X-ray spectroscopy (EDX).....	79
4.6 True porosity and bulk density of hydroxyapatite scaffold.....	80

LIST OF FIGURES

Figure		Page
1.1	Numbers of medical devices per year worldwide.....	2
1.2	Contribution of major countries in worldwide biomaterials production.....	2
1.3	Orthopedic biomaterials market growth strongest in U.S.....	3
1.4	Materials used in biomedical applications.....	3
2.1	hydroxyapatite structure ($\text{Ca}_{10}(\text{PO}_4)_6(\text{OH})_2$).....	8
2.2	XRD pattern of hydroxyapatite at Ca/P ratio 1.67 by mole.....	8
2.3	XRD pattern of hydroxyapatite at difference temperature.....	10
2.4	HAp crystals prepared hydrothermally at 200 °C for 24 hrs using moderate stirring. Room temperature pH of precursor slurries was 10. (a) Powders crystallized in 50 vol.% 2-propanol in H_2O (aq). (b) Powders crystallized with 1 wt.% KCl (aq).....	11
2.5	Hydroxyapatite synthesis by sol-gel method. (Wang et al., 2005).....	13
2.6	Synthesis of hydroxyapatite powder by Pechini method.....	14
2.7	The molecular formula of polyvinylpyrrolidone.....	15
2.8	The molecular formula of maltodextrin.....	24
2.9	Schematic diagram of spray drying process.....	24

LIST OF FIGURES (Continued)

		Page
3.1	Powder X-ray Diffraction (XRD) Bruker D2 PHASER.....	26
3.2	Mini spray dryer (BUCHI B-290).....	30
3.3	Scanning electron microscopy (SEM) JEOL JSM-6010LV.....	31
3.4	Particle size Distribution Analyzer (PSD), Horiba LA-950V2	32
3.5	Aspirator settings versus throughput.....	35
3.6	Conversion tables for spray drying parameters.....	36
3.7	Diagram of sintering process of hydroxyapatite scaffolds	39
3.8	Diagram of the first step : preparation of hydroxyapatite granules	40
3.9	Diagram of the second step : scaffold preparation	41
4.1	XRD pattern of hydroxyapatite raw material powder	42
4.2	Shows the particle stick in the wall of spray drying chamber.....	45
4.3	Scanning electron microscope of hydroxyapatite granule at inlet drying air temperature 220 °C, drying air flow rate 35 m ³ /h, slurry feed rate 5 ml/min, spraying air flow rate 357 l/h.....	46
4.4	Scanning electron microscope of hydroxyapatite granule at inlet drying air temperature 220 °C, drying air flow rate 35 m ³ /h, slurry feed rate 15 ml/min, spraying air flow rate 357 l/h.....	46

LIST OF FIGURES (Continued)

		Page
4.5	Scanning electron microscope of hydroxyapatite granule at inlet drying air temperature 220 °C, drying air flow rate 35 m ³ /h, slurry feed rate 10 ml/min, spraying air flow rate 357 l/h.....	47
4.6	Scanning electron microscope of hydroxyapatite granule at inlet drying air temperature 220 °C, drying air flow rate 35 m ³ /h, slurry feed rate 10 ml/min, spraying air flow rate 473 l/h.....	47
4.7	Scanning electron microscope of hydroxyapatite granule at inlet drying air temperature 220 °C, drying air flow rate 35 m ³ /h, slurry feed rate 10 ml/min, spraying air flow rate 601 l/h.....	48
4.8	Scanning electron microscope of hydroxyapatite granule at inlet drying air temperature 200 °C, drying air flow rate 35 m ³ /h, slurry feed rate 15 ml/min, spraying air flow rate 357 l/h.....	48
4.9	Scanning electron microscope of hydroxyapatite granule at inlet drying air temperature 220 °C, drying air flow rate 35 m ³ /h, slurry feed rate 20 ml/min, spraying air flow rate 357 l/h.....	49
4.10	Scanning electron microscope of hydroxyapatite granule at inlet drying air temperature 220 °C, drying air flow rate 32 m ³ /h, slurry feed rate 20 ml/min, spraying air flow rate 357 l/h.....	49
4.11	Scanning electron microscope of hydroxyapatite granule at inlet drying air temperature 220 °C, drying air flow rate 28 m ³ /h, slurry feed rate 20 ml/min, spraying air flow rate 357 l/h.....	50

LIST OF FIGURES (Continued)

		Page
4.12	Scanning electron microscope of hydroxyapatite granule at inlet drying air temperature 170° C, drying air flow rate 35 m ³ /h, slurry feed rate 15 ml/min, spraying air flow rate 357 l/h.....	50
4.13	Show graph of particle size distribution of hydroxyapatite granule at inlet drying air temperature 220 ° C, drying air flow rate 35 m ³ /h, slurry feed rate 5 ml/min, spraying air flow rate 357 l/h.....	51
4.14	Show graph of particle size distribution of hydroxyapatite granule at inlet drying air temperature 220 ° C, drying air flow rate 35 m ³ /h, slurry feed rate 15 ml/min, spraying air flow rate 357 l/h.....	52
4.15	Show graph of particle size distribution of hydroxyapatite granule at inlet drying air temperature 220 ° C, drying air flow rate 35 m ³ /h, slurry feed rate 10 ml/min, spraying air flow rate 357 l/h.....	52
4.16	Show graph of particle size distribution of hydroxyapatite granule at inlet drying air temperature 220 ° C, drying air flow rate 35 m ³ /h, slurry feed rate 10 ml/min, spraying air flow rate 473 l/h.....	53
4.17	Show graph of particle size distribution of hydroxyapatite granule at inlet drying air temperature 220 ° C, drying air flow rate 35 m ³ /h, slurry feed rate 10 ml/min, spraying air flow rate 601 l/h.....	53
4.18	Show graph of particle size distribution of hydroxyapatite granule at inlet drying air temperature 200 ° C, drying air flow rate 35 m ³ /h, slurry feed rate 15 ml/min, spraying air flow rate 357 l/h.....	54

LIST OF FIGURES (Continued)

		Page
4.19	Show graph of particle size distribution of hydroxyapatite granule at inlet drying air temperature 220 °C, drying air flow rate 35 m ³ /h, slurry feed rate 20 ml/min, spraying air flow rate 357 l/h.....	54
4.20	Show graph of particle size distribution of hydroxyapatite granule at inlet drying air temperature 220 °C, drying air flow rate 32 m ³ /h, slurry feed rate 20 ml/min, spraying air flow rate 357 l/h.....	55
4.21	Show graph of particle size distribution of hydroxyapatite granule at inlet drying air temperature 220 °C, drying air flow rate 28 m ³ /h, slurry feed rate 20 ml/min, spraying air flow rate 357 l/h.....	52
4.22	Show graph of particle size distribution of hydroxyapatite granule at inlet drying air temperature 170° C, drying air flow rate 35 m ³ /h, slurry feed rate 15 ml/min, spraying air flow rate 357 l/h.....	56
4.23	Hydroxyapatite scaffold before sintering.....	61
4.24	SEM image of hydroxyapatite scaffolds at hydroxyapatite to sodium chloride (NaCl) ratio 50 : 50 using prepared of sodium chloride 250 μm.....	61
4.25	SEM image of hydroxyapatite scaffolds at hydroxyapatite to sodium chloride (NaCl) ratio 50 : 50 using prepared of sodium chloride 325 μm.....	62

LIST OF FIGURES (Continued)

	Page
4.26 SEM image of hydroxyapatite scaffolds at hydroxyapatite to sodium chloride (NaCl) ratio 50 : 50 using prepared of sodium chloride 400 μm	62
4.27 SEM image of hydroxyapatite scaffolds at hydroxyapatite to sodium chloride (NaCl) ratio 60 : 40 using prepared of sodium chloride 250 μm	63
4.28 SEM image of hydroxyapatite scaffolds at hydroxyapatite to sodium chloride (NaCl) ratio 60 : 40 using prepared of sodium chloride 325 μm	63
4.29 SEM image of hydroxyapatite scaffolds at hydroxyapatite to sodium chloride (NaCl) ratio 60 : 40 using prepared of sodium chloride 400 μm	64
4.30 Hydroxyapatite scaffold after sintered at 1300 °C for 1 hr.....	65
4.31 XRD pattern of hydroxyapatite after sintering at 1300°C.....	66
4.32 SEM photo of sintered hydroxyapatite scaffolds formed by mixing sodium chloride particle of 250 μm with spray dried hydroxyapatite granules at mixing ratio 50:50.....	67

LIST OF FIGURES (Continued)

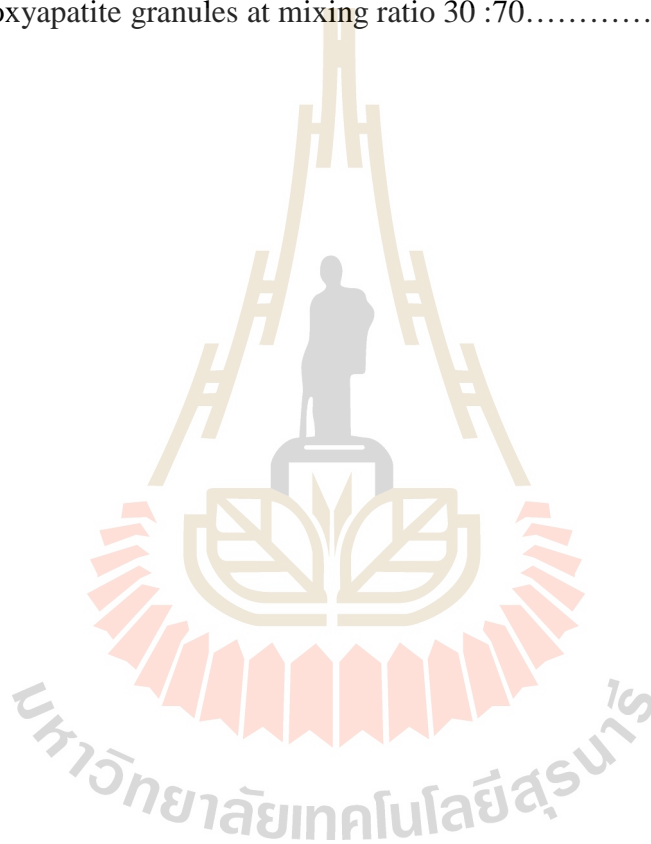
		Page
4.33	SEM photo of sintered hydroxyapatite scaffolds formed by mixing sodium chloride particle of 325 μm with spray dried hydroxyapatite granules at mixing ratio 50:50.....	68
4.34	SEM photo of sintered hydroxyapatite scaffolds formed by mixing sodium chloride particle of 400 μm with spray dried hydroxyapatite granules at mixing ratio 50:50.....	69
4.35	SEM photo of sintered hydroxyapatite scaffolds formed by mixing sodium chloride particle of 250 μm with spray dried hydroxyapatite granules at mixing ratio 60:40.....	70
4.36	SEM photo of sintered hydroxyapatite scaffolds formed by mixing sodium chloride particle of 325 μm with spray dried hydroxyapatite granules at mixing ratio 60:40.....	71
4.37	SEM photo of sintered hydroxyapatite scaffolds formed by mixing sodium chloride particle of 400 μm with spray dried hydroxyapatite granules at mixing ratio 60:40.....	72

LIST OF FIGURES (Continued)

		Page
4.38	SEM photo of sintered hydroxyapatite scaffolds formed by mixing sodium chloride particle of 250 μm with spray dried hydroxyapatite granules at mixing ratio 40:60.....	73
4.39	SEM photo of sintered hydroxyapatite scaffolds formed by mixing sodium chloride particle of 325 μm with spray dried hydroxyapatite granules at mixing ratio 60:40.....	74
4.40	SEM photo of sintered hydroxyapatite scaffolds formed by mixing sodium chloride particle of 400 μm with spray dried hydroxyapatite granules at mixing ratio 60 : 40.....	75
4.41	SEM photo of sintered hydroxyapatite scaffolds formed by mixing sodium chloride particle of 250 μm with spray dried hydroxyapatite granules at mixing ratio 30:70.....	76
4.42	SEM photo of sintered hydroxyapatite scaffolds formed by mixing sodium chloride particle of 325 μm with spray dried hydroxyapatite granules at mixing ratio 30 :70.....	77

LIST OF FIGURES (Continued)

	Page
4.43 SEM photo of sintered hydroxyapatite scaffolds formed by mixing sodium chloride particle of 400 μm with spray dried hydroxyapatite granules at mixing ratio 30 :70.....	78



CHAPTER I

INTRODUCTION

From past to present scientists have tried to find a way to increase human lifespan and make people less vulnerable to the illnesses. Technological advances are becoming ever more lifelong. However, we still have to suffer from the diseases and degeneration of the body with age. Changes that occur in body's tissues and organs affect the function of all body. Nowadays, materials or equipment made of synthetic or semi-synthetic materials are frequently used to assist in the treatment, enhancement, or replacement of organs and tissues of the damaged body. We call these materials medical or biological materials such as hip-knee prosthesis, dental implants, bone graft, etc. Each year many millions of pieces of biomaterials are used around the world, as shown in Figure 1.1 [1]. . The total value is more than \$ 5,000 million per year, as illustrated in Figure 1.2 [2]. The contribution of USA, Japan, Germany and other European countries accounts for \$ 3,900 million per year. The market in the United States has used a wide range of biological materials, as shown in Figure 1.3.

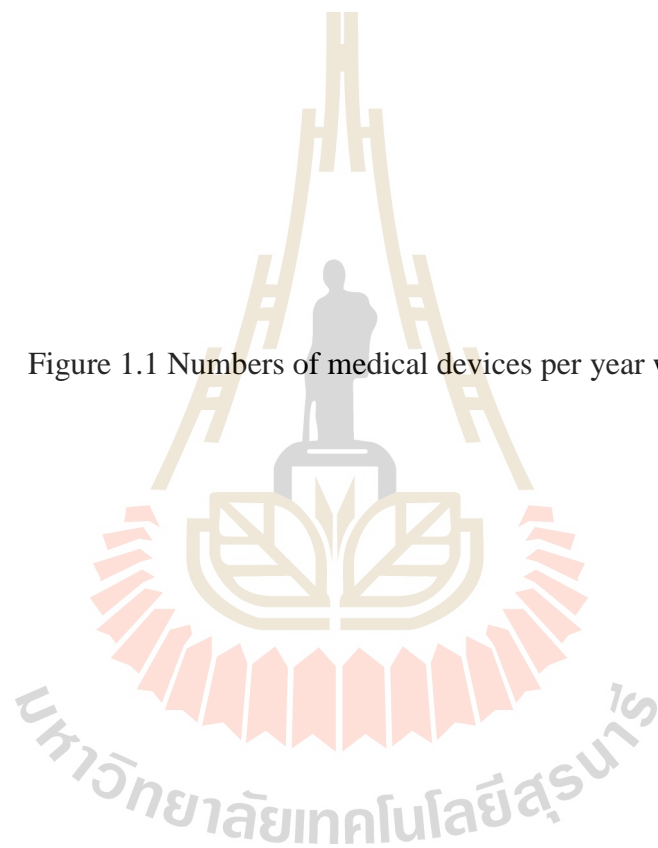


Figure 1.1 Numbers of medical devices per year worldwide [1]

Figure 1.2 Contribution of major countries in worldwide biomaterials production [2]

Figure 1.3 Orthopedic biomaterials market in U.S.

A large variety of polymer, metal, ceramic and composite materials are used as Biomaterials as show in figure 1.4

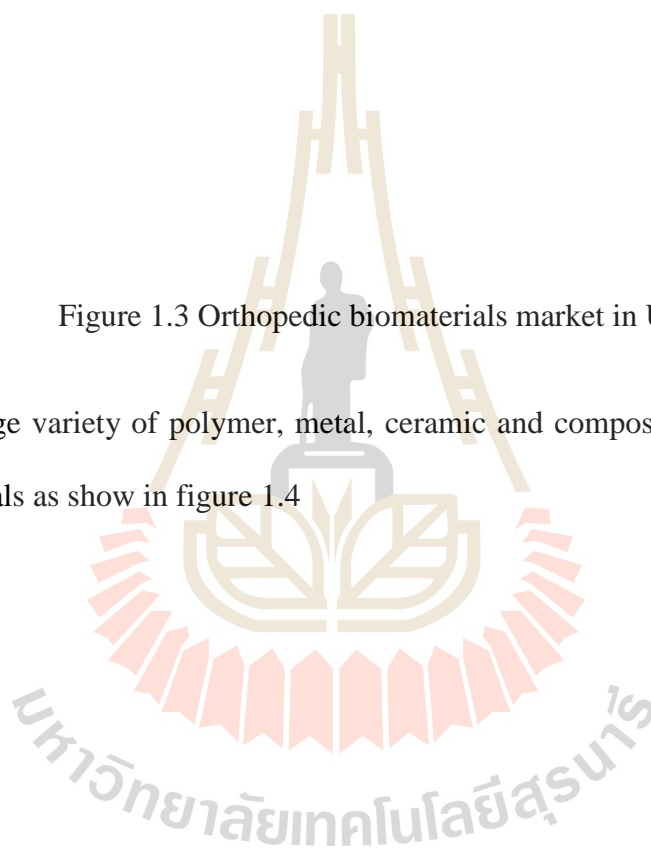


Figure 1.4 Materials used in biomedical applications.

Recently, many researchers have tried to develop a bone replacement scaffold for use in orthopedic implants with properties similar to real human bone. Hydroxyapatite, HA [$\text{Ca}_{10}(\text{PO}_4)_6(\text{OH})_2$], is the popular bioceramic material utilized in fabrication of bone replacement scaffolds and bone implants because it has chemical structure and physical properties similar to the mineral found in human bones and teeth. In the field of tissue engineering, the bone replacement scaffold requires materials with composition and porosity close to human. The fabrication process is one of key parameters to control effectively properties of the bone replacement scaffold. The hydroxyapatite scaffolds can be fabricated by several processes such as leaching, gas expansion, emulsion freeze-drying, thermally induced phase separation, 3D printing, etc. The hydroxyapatite scaffolds are required to have the porous structure with interconnected pores of different sizes for cell growth and cell penetration. The porogen leaching technique is an easy process to fabricate the hydroxyapatite scaffold. This technique uses the chloride particles such as NaCl, CaCl, etc. to generate the porous structure. It can be applied to form large pores with size controlled by the size of chloride particles. Then, agglomerates with small pores could be produced in spray drying of a slurry of fine particles. Moreover, connected mesopores are formed among agglomerates during the compaction stage.

In this research, the preparation of hydroxyapatite scaffolds with interconnected multi-size porous structure is investigated using the mixture of spray dried agglomerates of fine particles and sodium chloride particles of various sizes as a porogen. Thus, the difference in pores sizes come from voids inside granules, pores in granule packing and pores formed after sodium chloride burn out.

1.1 Research objective

The research objectives of the present thesis are as follows:

1. To investigate the optimum conditions for preparation of spray dried granules with the uniform size distribution, spherical shape and good flowability.
2. To design the porous structure of scaffold by using the mixture of spray dried granules and sodium chloride particles as the porogen with different particles sizes and various mixing ratios.

1.2 Scope and limitation of thesis

The scope and limitation of thesis can be summarized as follows:

1. Study spray drying parameters such as the inlet temperature of drying air, slurry feed rate, spraying air flow rate and aspirator rate that will be adjusted to obtain granules of uniform size distribution and spherical shape.
2. The scaffold will be prepared using spray-dried hydroxyapatite granules.
3. The scaffold pore size will be adjusted by adding sodium chloride with different particles sizes and various mixing ratios.
4. The characteristics of sintered scaffold such as the morphology, porosity, pore size, density will be analyzed.

1.3 Expected results

The expected results are summarized as follows:

1. The optimum spray drying conditions will be determined for the production of spray dried granules with good flowability, morphology and narrow size distribution.
2. The scaffolds with different pore sizes will be prepared by using hydroxyapatite granules and sodium chloride particles.
3. The scaffolds of improved strength will be prepared using hydroxyapatite granules.



CHAPTER II

LITERATURE REVIEW

2.1 Materials

2.1.1 Hydroxyapatite ($\text{Ca}_{10}(\text{PO}_4)_6(\text{OH})_2$)

Hydroxyapatite is a calcium phosphate which is the primary mineral component of bone and similar to the human hard tissue in composition and morphology. It has the physical attributes of stability, inertness and biocompatibility. However, synthetic hydroxyapatite has a limitation in implant application due to poor mechanical strength including low strength and fracture toughness when compare with human bone. The difference in mechanical strength results from the minor descriptions in composition and microstructure between real human bone and synthetic hydroxyapatite. Synthetic hydroxyapatite commonly has isotropic structure, i.e. the properties do not depend on the direction, and larger grains than those of real bone. The real human bone is composed of organic collagen and biological apatite.

2.1.1.1 Hydroxyapatite Structure

The mineral apatite can be represented by formula $\text{M}_{10}(\text{ZO}_4)_6\text{X}_2$ (or $\text{M}_5(\text{ZO}_4)_3\text{X}$) and the formula of calcium hydroxyapatite is $\text{Ca}_{10}(\text{PO}_4)_6(\text{OH})_2$. The hydroxyapatite has a hexagonal structure with lattice

parameters $a = b = 9.43$, $c = 6.88$ angstrom and angles $\alpha = \beta = 90^\circ$, $\gamma = 120^\circ$, as shown in Figure 2.1.

Figure 2.1 hydroxyapatite structure ($\text{Ca}_{10}(\text{PO}_4)_6(\text{OH})_2$).

2.1.1.2 Composition of hydroxyapatite

Pure hydroxyapatite composes of calcium (Ca) 39.68 wt%, phosphate 18.45 wt% with a stoichiometric Ca/P ratio of 1.67 by mole or 2.151 by weight. If the Ca/P ratio have 1.67 by mole XRD pattern as show in the figure 2.2.

Figure 2.2 XRD pattern of hydroxyapatite at Ca/P ratio 1.67 by mole

2.1.1.3 Synthesis of hydroxyapatite

The varieties of synthesis technique for hydroxyapatite have 5 varieties in the present included (a) solid state reaction, (b) Precipitation, (c) Hydrothermal, (d) sol-gel, (e) the pechini method

(a) Solid state reaction

Preparation of solid state reaction of the powder method based on a chemical reaction from a mixture of solid starting materials. It is widely used in the preparation of complexes of oxides. Use carbonates, nitrate, sulfate, acetate and oxalate as the starting material. For example, the synthesis of the ceramic powder material. Structure of Hydroxyapatite ($\text{Ca}_{10}(\text{PO}_4)_6(\text{OH})_2$, HAp) and β -tri-calcium phosphine ($\text{Ca}_3(\text{PO}_4)_2$, -TCP). The reaction between Brucite (Brushite, $\text{CaHPO}_4 \cdot 2\text{H}_2\text{O}$) and calcium carbonate (CaCO_3) equation 1 and 2



Brucite and calcium carbonate were mixed using wet ball milling technique and the solution was dried. After that, the solid mixture was heated up and reaction occur between different substrates. Finally, calcination process was carried out to obtain the hydroxyapatite powder.

Figure 2.3 XRD pattern of hydroxyapatite at difference temperature

(a) 1000°C/1hr, (b) 1000°C/4hrs, (c) 1100°C/2hr, (d)

1200°C/2hr

(b) Precipitation

Precipitation is a chemical technique. It was the wet quantitative analysis was used to prepare compounds of inorganic salts. Sedimentation the molecules or ions dissolved in the solution separation of the solution by added optimize participant slowly in moderation or change the temperature or pressure to reduce. Reduce the system's solubility. The sedimentation process consists of the following mechanisms is nucleation and growth. Molecules or ions of foreign matter are mixed in the solution by sticking the surface of the atomic particle. It is also important to make the sediment a shape-dependent (anisotropy).

(c) Hydrothermal

The hydrothermal techniques is crystallizing substances from high-temperature aqueous solutions at high vapor pressures. Hydrothermal hydrolysis of the substrate is in the form of $\text{Ca}(\text{NO}_3)_2$, $(\text{NH}_4)_2\text{HPO}_4$, $\text{NH}_4\text{H}_2\text{PO}_4$, 29% NH_4OH and 9% HNO_3 . This technique get to quantity and quality of high hydroxyapatite powder and have the needle-structure is wide about 20-40 nm and length about 100-160 nm.

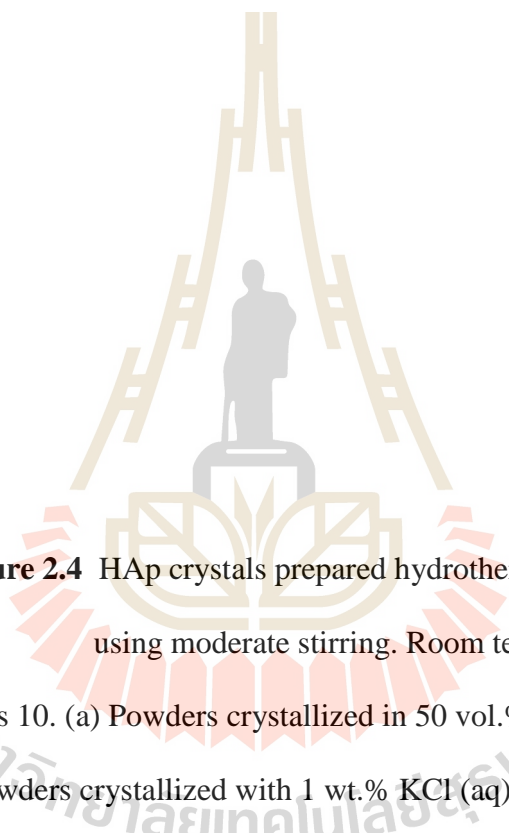


Figure 2.4 HAp crystals prepared hydrothermally at 200 °C for 24 hrs using moderate stirring. Room temperature pH of precursor slurries was 10. (a) Powders crystallized in 50 vol.% 2-propanol in H_2O (aq). (b) Powders crystallized with 1 wt.% KCl (aq). (Riman et al., 2002) (d) Sol-gel

Sol-gel preparation is a chemical process it widely of most popular. This is a very effective technique for producing quality work pieces and can used in the production various such as Catalysis, Absorbents, Thin films, Coating, Biotechnology (Biomaterials). Sol-gel method is as follows;

1. Prepare sols from particle size smaller than 0.1 μm .

2. Change the concentration by evaporating some liquid or leave it for a long time or add appropriate electrolyte to bonding of a bond is a continuous three-dimensional network similar to the polymerization process (Polymerization).
3. Evaporates the liquid leave from the gel (Dehydration). The strength of the gel will prevent the atoms from moving.
4. Calcination gel for change to the compounds.

The powder produce from sol-gel method is a very fine particle in the range of 20 to 50 nm and has a very high surface area. The sintering can be done at low temperatures. Synthesis of hydroxyapatite powder by sol-gel method as show in figure 2.5 the substrate used in the form of P_2O_5 , C_2H_5OH , $Ca(NO_3) \cdot 4H_2O$ (Wang et al., 2005) based on wet chemical reactions.

Figure 2.5 Hydroxyapatite synthesis by sol-gel method. (Wang et al., 2005)

(e) The pechini method

The pechini method or the polymerized complex method was derived from the traditional sol-gel process in 1967. The pechini is suitable for thin film preparation. After that, improved for preparation powders.

Pechini to show the formation compounds of alkali metals, alkali earths, transition metal, and some non-metallic substances. These substances react with organic compounds such as citric acid and added poly-alcohol such as polyethylene glycol to bond between metals and organic compounds with

polyesterification is get to the gel formation in the mixture. After drying the gel, the particles are agglomerate and have a size less than the micrometer.

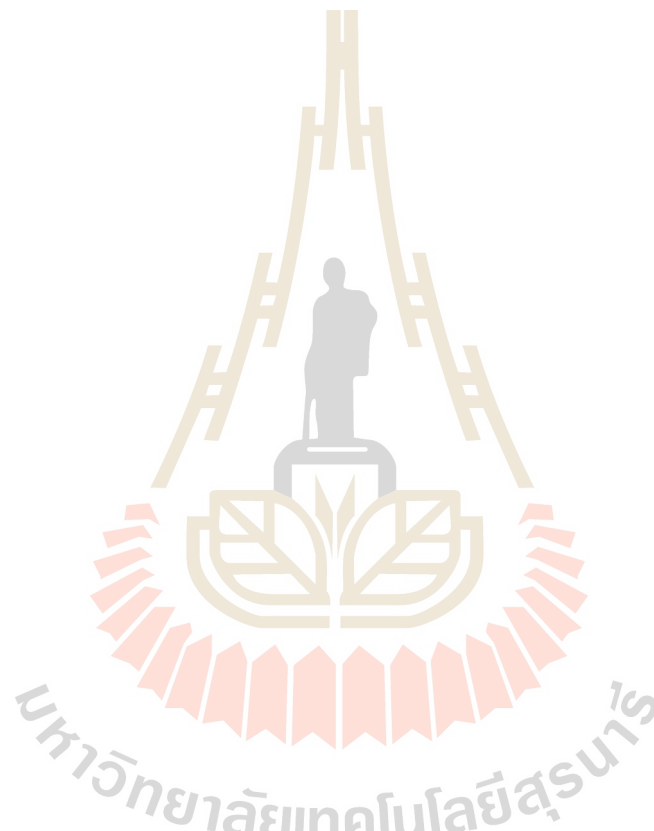


Figure 2.6 Synthesis of hydroxyapatite powder

2.1.2 Polyvinylpyrrolidone (PVP)

Polyvinylpyrrolidone is a water-soluble polymer made from the monomer. It is soluble in water and other polar solvents. PVP is soluble in water and other polar solvents. For example, it is soluble in various alcohols, such as methanol and ethanol, as well as in more exotic solvents like the deep eutectic

solvent formed by choline chloride and urea. It can be used as a binder in many pharmaceutical, co-solvent of tablets, granules, and injection, as the dispersant agent of liquid preparations.

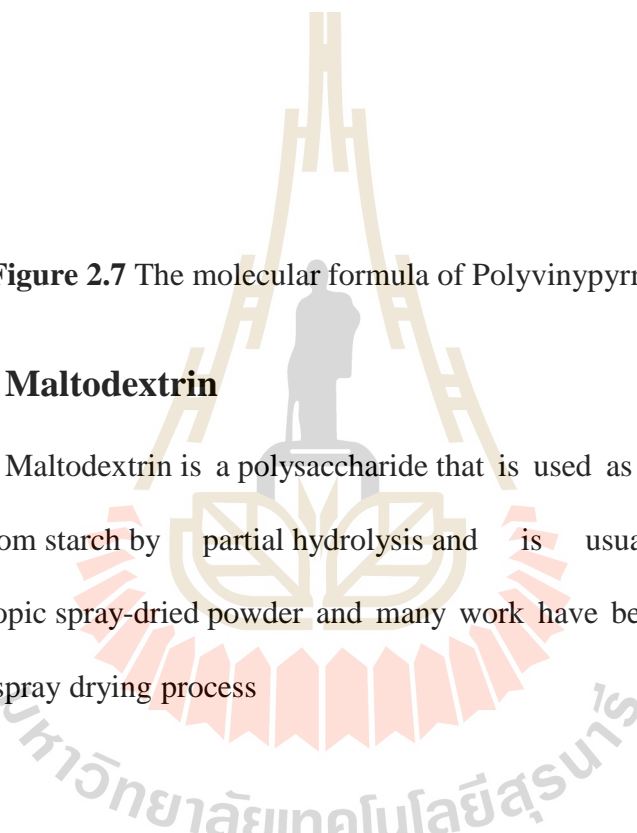


Figure 2.7 The molecular formula of Polyvinylpyrrolidone.

2.1.3 Maltodextrin

Maltodextrin is a polysaccharide that is used as a food additive. It is produced from starch by partial hydrolysis and is usually found as a white hygroscopic spray-dried powder and many work have been used maltodextrin as a binder in spray drying process

Figure 2.7 The molecular formula of maltodextrin

Banu et al. (2014) studied the effect of spray drying condition on the physical properties of spray dried maltodextrin. In the spray dried process was used maltodextrin solution 25%. The physical properties of maltodextrin powders were investigated. The results showed the spray drying could be produce smaller particles. The bulk, tapped and particle densities of spray dried maltodextrin were <350 , <575 and $<1310 \text{ kg m}^{-3}$, respectively. These values are ~~an~~ indicated that maltodextrin obtained the moderate porosity.

Kumer et al. (2016) prepared hydroxyapatite by three-dimensional porous scaffolds by using two different kind of binders (maltodextrin and sodium alginate) and fabricated using the extrusion method of three-dimensional. The result showed the fracture under compressive loading, with hydroxyapatite-alginate scaffolds shown a higher compressive strength ($9.5 \pm 0.5 \text{ MPa}$) than hydroxyapatite-maltodextrin scaffolds ($7.0 \pm 0.6 \text{ MPa}$).

R.Chumnanklang et al. (2016) fabricated hydroxyapatite by 3D printing and study the effect of binder concentration in pre-coat particle in part strength. The hydroxyapatite preparation by spray dried ~~at~~ with difference concentration of maltodextrin binder. The concentration of binder was influenced to the properties of both green and sintered samples. It was observed that the sintered strength of hydroxyapatite are increased with increasing of green strength due to increasing of the binder concentration and pre-coated particle size.

2.2 Bone replacement scaffolds

Bone is a natural composite of collagen and hydroxycarbonate apatite with 10–30 % porous hard outer layer, cortical bone, and 30–90% porous interior, cancellous bone. The mechanical properties of cortical and cancellous bones were found to be different. The scaffolds are used for replacement of cancellous

bone. The key factors of an ideal bone scaffold for bone tissue engineering are (I) macro- (pore size $>100\ \mu\text{m}$) and microporosity (pore size $< 20\ \mu\text{m}$), (II) interconnected open porosity for in vivo tissue in-growth, (III) sufficient mechanical strength and controlled degradation kinetics for proper load transfer to the adjacent host tissue, (IV) initial strength for safe handling during sterilizing, packaging, transportation to surgery, as well as survival through physical forces in vivo, and (V) sterile environment for cell seeding (Susmita et al., 2012). In the field of tissue engineering, it is well known that scaffolds, appropriately designed in terms of structure and properties play an important role to direct and provide support to the growth of cells as well as their migration around surrounding tissue. The property requirements of scaffolds include;

- (I) Biocompatibility is the first property requirement of bone scaffolds. The scaffolds it should be biocompatible for cells to adhere, function normally, migrate onto the surface and through the scaffold, proliferate and form matrix on its surface and pore. After implantation, the scaffold must elicit immunogenicity reaction to prevent it causing such a severe inflammatory response that it might reduce healing or cause rejection by the body.

- (II) The material should induce strong bone bonding, resulting in osteoconduction and osteoinduction.

Rate of new tissue formation and biodegradability, the scaffolds must be biodegradable when degradation and without interference with other organ when able to exit body.

- (III) Mechanical properties are important properties for bone scaffolds. The mechanical properties of an ideas should be similar to those of host bone and proper weight transfer. However, the bone have the mechanical properties vary widely; Young's modulus of cortical bone is between 15 and 20 GPa and that of cancellous bone is between 0.1 and 2 GPa. Compressive strength varies between 100 and 200 MPa for cortical bone, and between 2 and 20 MPa for cancellous bone. The mechanical strength of the scaffolds should be adequate enough to provide mechanical constancy in load bearing sites prior to regeneration of new tissue and its must be strong enough to allow surgical handing during.

- (IV) porous structure and pore size of more than 100 μm for cell penetration, tissue ingrowth and vascularization (see also Table 1)

Table 2.1 Pore size distribution for an ideal scaffold in bone tissue engineering applications (Tripathi et al., 2012).

Pore size (μm)	Biological function
<1	Protein interaction, responsible for bioactivity
1-20	Cell attachment and orientation of cellular growth
100-1000	Cellular growth and bone ingrowth
>1000	Shape and functionality of implant

Narbat et al. (2006) prepared the hydroxyapatite (HA) and gelatin (GEL) composite scaffolds to mimic the mineral and organic component of natural bone. The composite HA-GEL scaffolds were prepared by solvent casting method. The composite spectrums are similar to the spectra of real bone. The measurements of scaffold mechanical properties confirmed that the compressive modulus increases at higher HA content. The scaffold pores were interconnected and their sizes ranged from 80 to 400 μm . The scaffold porosity was 70% and density 1.17 g/cm^3 .

Swain et al. (2015) developed macro porous hydroxyapatite scaffolds by insertion of hydroxyapatite powder into the PVA-PEG hydrogel and investigated the effect of concentration and molecular weight of polyethylene glycol (PEG) particle on strength, porosity and pore size of synthesized scaffold. They synthesized hydroxyapatite from $\text{Ca}(\text{Na}_3)_24\text{H}_2\text{O}$ and $(\text{NH}_4)_2\text{HPO}_4$ by co-precipitation method and stabilized phase at 1250°C. The scaffold was prepared using polyethylene glycol

(PEG) cross linked with polyvinyl alcohol (PVA). The fabricated scaffold has 70% volume porosity with strength 4.2 MPa and pore within the range \square 70-100 μ m.

Several materials have been used as scaffold material such as metal, ceramic, glass, polymer and composites. The examples of scaffold materials are summarized below:

(I) Metallic scaffolds. Ti, Mg scaffolds possess high compressive strength and excellent fatigue resistance, but they are non-biodegradable. However, there is a concern about the metal ion release.

(II) Bioglass scaffolds. When tested under in vitro conditions, 70% porous 3D bioglass scaffold with 300–400 μ m pore size showed hydroxyl-carbonate apatite (HCA) layer formation on the surface that significantly enhances the osteoblast activity. The HCA layer also adsorbs protein and facilitates new bone formation in vivo. (III) Polymeric scaffolds. These scaffolds are both bioactive and biodegradable. Generally, the natural polymers such as collagen, fibrin, alginate, silk, hyaluronic acid, and chitosan are used for bone tissue engineering application. In additions, the production processes are flexible and easily to tailor (Bose et al., 2012).

(IV) Ceramic scaffolds such as calcium phosphate (CaPs) based bioactive ceramic and hydroxyapatite scaffolds. They possess good biocompatibility due to their composition which is similar to the natural bone.

(V) Composites made from two or more distinctly different materials such as ceramics and polymers. Development of an interconnected CaP-polymer scaffold takes advantages of both CaPs and polymers to meet the mechanical and physiological requirements of the host tissue. Polymer in CaP scaffolds could increase the toughness and compressive strength similar to bone. Similarly, mechanical

integrity and bioactivity of polymers can be improved by adding CaP (Son et al., 2011). Hydroxyapatite is one of the ceramic materials that provides biocompatibility. Hydroxyapatite is a form of apatite mineral with the chemical formula $\text{Ca}_{10}(\text{PO}_4)_6(\text{OH})_2$. The needle-like crystals form the hydroxyapatite crystal structure. Hydroxyapatite possesses an excellent biocompatibility due to chemical and physical resemblance to the mineral constituents of human bones and teeth. Hydroxyapatite has been used in several studies as the bone replacement material. However, pure hydroxyapatite has limitations due to their poor mechanical strength and fracture toughness in comparison with the human bone. Therefore, it could only be utilized for non-load-bearing implants applications.

2.4 Scaffold fabrication

Recently, several techniques have been developed to fabricate tissue engineering scaffolds, including porogen leaching, gas expansion, emulsion freeze-drying, thermally induced phase separation, 3D printing, etc. In this work is used to prepare the porogen leaching technique, because this technique provides easy control of the pore structure in comparison with other techniques. Sodium chloride (NaCl) was utilized in the present work as a porogen (Tran et al., 2011). Sodium chloride, also known as salt, common salt, table salt or halite, is an ionic compound with the chemical formula NaCl, representing 1:1 ratio of sodium and chloride ions. In the preparation process, NaCl will be burnout over the leaching technique to remove the porogen at low temperature before sintering at high temperature. Nevertheless, the porous scaffold is usually fabricated by casting biomaterials with porogen followed by washing out the porogen by aqueous solution. The scaffold pore size, porosity and

pore morphology can be controlled by the properties of porogen. However, this technique may cause a problem of residual porogen in scaffold, which may lead to poor pore interconnectivity and harm the cell seeding.

2.5 Multiscale porous scaffold

In tissue engineering, cell and tissue will respond to growth in the pore of different size (see also Table 1). Therefore, the porous structure of scaffolds must be designed to include interconnected pores of different sizes. For example, in hierarchical scaffolds, the macropores (150–500 μm) maintain the structural stability of scaffolds, support cell proliferation, extra cellular matrix (ECM) deposition and tissue formation. The micrometer-scale (1–50 μm) pores are critical for nutrient diffusion and vascularization. Du et al. (2014) studied the macro porous polycaprolactone (PCL) nanofibrous scaffolds with multiscale pore distributions (macro-micro–nano) fabricated by a modified phase separation technique. The nanofiber morphology and pore structure were controlled by polymer concentration and phase separation temperature. Their experimental results confirmed that scaffolds of good nanofibrous structure and morphology as well as of high porosity were produced using low polymer concentration. Multiscale porous structure of scaffold was generated including nanometer-scale pores (50-500 nm.) formed among nanofibers, macrometer-scale (1-10 μm), and micrometer-scale pores (300-800 μm).

2.6 Hydroxyapatite granules by spray drying

Spray drying is a universal method for granule generation. It is widely used because of its advantages, including the fact that it is a simple process. The

spray-dried granules of controlled morphology including doughnut shape, solid sphere or hollow spheres can be manufactured by adjusting the nozzle diameter, inlet air temperature, atomized pressure, slurry concentration and feed rate, etc.

Spray drying is a method of producing a dry powder from a liquid or slurry feed by rapid drying of droplet spray with a hot gas. This is the preferred method of drying of many thermally-sensitive materials such as foods and pharmaceuticals. A consistent particle size distribution is a reason for using spray drying for manufacturing of some industrial products such as catalysts. Hot air is drying medium; however, if the liquid is a flammable solvent such as ethanol or the product is oxygen-sensitive then nitrogen is used. The particle size is an important property of spherical hydroxyapatite granules. There are many advantages in reducing the granule size of the spherical hydroxyapatite material. The smaller the granule size, the higher the specific surface area and the higher the bonding capacity. In addition, the mechanical properties of a packed material can be improved by reducing the granule size, resulting in larger contacting surface areas, and thereby greater friction forces between granules. Furthermore, a uniform packing is expected to have a homogenous pore size distribution (Luo and Nieh., 1996). Moreover, the hydroxyapatite microspheres usually are meso porous in nature and this porous structure could be contributed to the multiscale pore structure of scaffold (Padmanabhan et al., 2014).

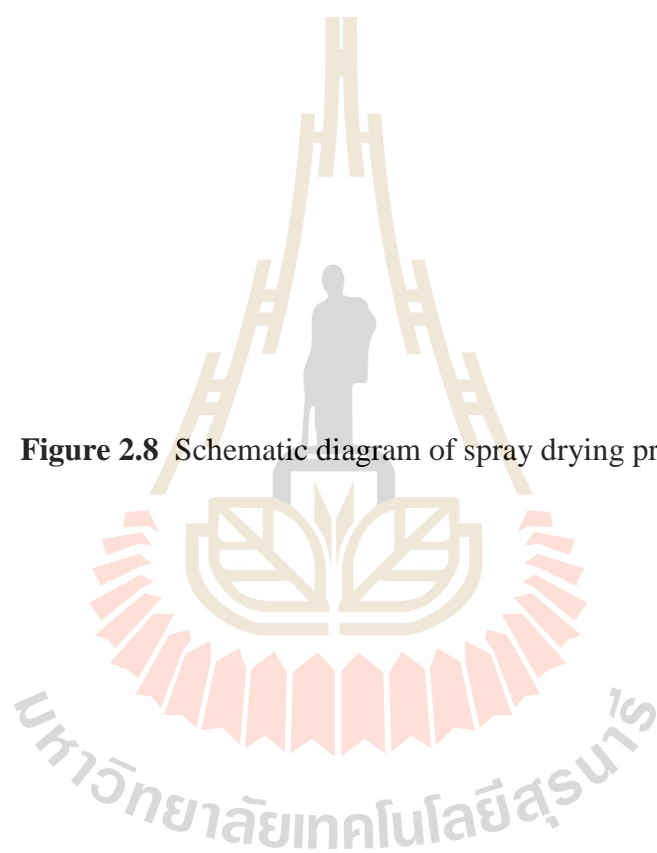


Figure 2.8 Schematic diagram of spray drying process .

CHAPTER III

EXPERIMENTAL PROCEDURE

3.1 Sample preparation and analytical equipment

Sample preparation and analytical equipment used for the preparation samples and their characterization are summarized in Table 1.

Table 3.1 Sample preparation and analytical equipment.

Sample preparation and Analytical Equipment	Company	Type/Model
X-ray Diffraction (XRD)	Bruker	D2 Phases
Mini spray dryer	BUCHI	B290
Scanning Electron Microscope (SEM)	JEOL	JSM-6010LV
Particle size Distribution Analyzer (PSD)	Horiba	LA-950V2
Ball Mill	P.S.C.M.	-
Furnace (1400 °C)	Carbolite	RHF 15/35
Oven	Binder	WTB
Sieve	Retsch	-
Ultrasonic	Scientific	950

I. Powder X-ray Diffraction (XRD)

Start with samples preparation and then characterization. X-ray diffraction used for characterization raw materials powders. X-ray diffraction is a standard technique for material characterization to obtain micro structural information for crystalline and non-crystalline materials. This non-destructive method could provide information such as crystal structure, lattice parameter, crystal size, composition etc. which are useful for ceramics, metal alloys, semiconductors, polymer, nano-materials research. **X-ray source**

- Ceramic Cu X-ray tube
- 30 kV/ 10 mA

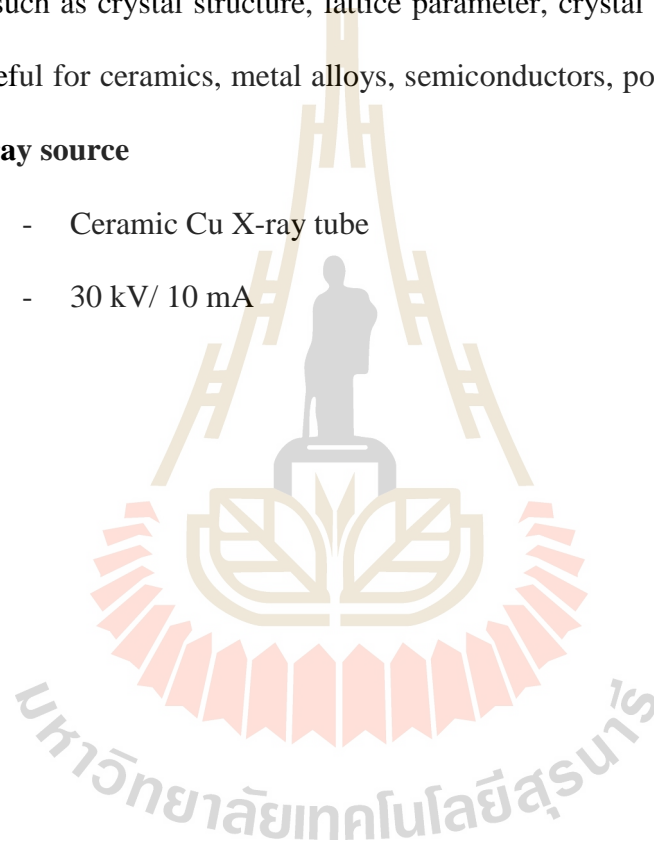


Figure 3.1 Powder X-ray Diffraction (XRD) Bruker D2 PHASER

I. Mini spray dryer (BUCHI B-290)

Spray dryer (BUCHI B-290) used for preparation the hydroxyapatite granules for fabrication hydroxyapatite scaffolds. A nozzle with diameter 0.7 mm, maximum temperature input 220 °C, airflow maximum 35 m³/h and evaporating capacity 1.0 l/h H₂O. Four drying parameters were adjusted in our equipment

including inlet drying air temperature, drying air flow rate, slurry feed rate and spraying air flow rate.

a. Inlet air temperature / Outlet temperature.

Inlet temperature is being the temperature of the heating drying air. The drying air is sucked in over a heater by the aspirator. The heated air temperature is measured prior to flowing into the drying chamber. When spray drying a solution, emulsion or dispersion the solvent is removed by vaporization.

The temperature of the air with the solid particles before entering the cyclone is designated as the outlet temperature. This temperature is the resulting temperature of the heat and mass balance in the drying cylinder and thus cannot be regulated. Due to the intense heat and mass transfer and the loss of humidity, the particles can be regarded to have the same temperature as the gas. Thus, as a rule of thumb is: outlet temperature = maximum product temperature.

The outlet temperature is the result of the combination of the following parameters:

- Inlet temperature
- Aspirator flow rate (quantity of air)
- Peristaltic pump setting
- Concentration of the material being sprayed

b. Drying air flow rate.

The drying air is sucked through the device by the aspirator motor creating under pressure conditions. By regulating the aspirator speed, the amount of heated drying air can be increased or decreased. If the system is running in the sucking mode, a slight under pressure will take effect in the spray dryer. Because the amount of

energy available for vaporization changes when the amount of drying air is increased or decreased, the aspirator speed setting has a significant effect on the drying performance of the device.

The optimum setting must be determined experimentally using the following guidelines:

High aspirator speed → higher degree of separation in the cyclone.

Lower aspirator speed → lower residual moisture content

c. Slurry feed rate or pump performance.

The peristaltic pump feeds the spray solution to the nozzle. The pump's speed affects the temperature difference between the inlet temperature and the outlet temperature. The pump rate directly corresponds to the inlet mass. The higher the throughput of solution, the more energy is needed to evaporate the droplet to particles. Thus, the outlet temperature decreases. The limitation of the pump is when the particles are not dry enough resulting in sticky product or wet walls in the cylinder. The pump throughput is also dependent upon various factors such as the viscosity of the spray solution and tubing diameter.

d. Spraying air flow rate.

The spray flow rate is the amount of compressed air needed to disperse the solution, emulsion or suspension. A spray flow rate can be set to between 300 and 800 l/h on the device. The table below gives a correlation of the flow meter and the gas throughput. The particle size of the final product can be influenced by the spray flow rate setting, Show in Table.4

Table 3.2 Parameter of spray flow rate setting for control size of the final product.

Height (mm)	liter /hour	Pressure drop (bar)	Actual volume flow (at standard temperature and pressure) in liters / hour
5	84	-	-
10	138	-	-
15	192	-	-
20	246	0.15	282.90
25	301	0.18	355.18
30	357	0.23	439.11
35	414	0.3	538.20
40	473	0.41	666.93
45	536	0.55	830.80
50	601	0.75	1051.75
55	670	1.05	1373.50
60	742	1.35	1743.70
65	819	1.80	2293.20

The table gives a correlation between indicated height and volume throughput. The nozzle has a certain pressure drop which increases with higher gas bar. As gas volume strongly corresponds to the actual pressure, the also contains a row for the effective volume flow, determined in spray process with water.

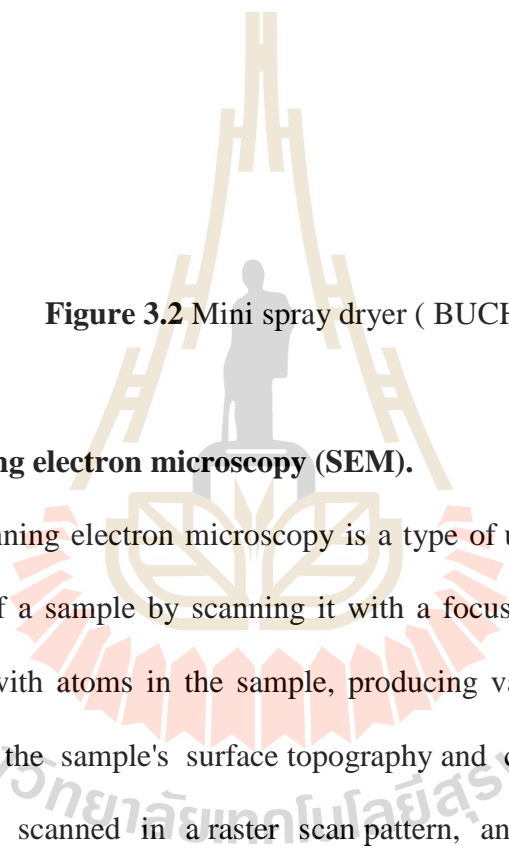


Figure 3.2 Mini spray dryer (BUCHI B-290)

III. Scanning electron microscopy (SEM).

Scanning electron microscopy is a type of utilized an microscope that produces images of a sample by scanning it with a focused beam of electrons. The electrons interact with atoms in the sample, producing various signals that contain information about the sample's surface topography and composition. The electron beam is generally scanned in a raster scan pattern, and the beam's position is combined with the detected signal to produce an image. Specimens can be observed in high vacuum, in low vacuum, in wet conditions (in environmental SEM), and at a wide range of cryogenic or elevated temperatures. The most common SEM mode is detection of secondary electrons emitted by atoms excited by the electron beam. The number of secondary electrons that can be detected depends, among other things, on specimen topography. By scanning the sample and collecting the secondary electrons

that are emitted using a special detector, an image displaying the topography of the surface is created. The scanning electron microscope (SEM) JEOL JSM-6010LV used in the present study figure.3 include

- Electron Optics
- Tungsten filament
- High tension 0.5 kV- 20 kV
- Resolution high-vacuum 4 nm at 20 kV, 15 nm at 1 kV
- Resolution low-vacuum 5 nm at 20 kV
- Magnification 8x – 300,000x
- Beam current 1 pA to 300 nA
- Auto filament alignment
- Beam blanking

Figure 3.3 Scanning electron microscopy (SEM) JEOL JSM-6010LV.

IV. Particle size Distribution Analyzer (PSD)

HORIBA LA-950V2 can measure particle size rang 0.01 – 3,000 microns, widest wet dynamic range on the market of 300,000 to 1 and small particle sensitivity: accurately measure 30 nanometer diameter particles

Figure 3.4 Particle size Distribution Analyzer (PSD), Horiba LA-950V2

3.2 Materials

Materials used in experiments are show in Table 3.3.

Table 3.3 Materials used in experiments

Materials	Chemical formula	Company
Hydroxyapatite	$\text{Ca}_{10}(\text{PO}_4)_6(\text{OH})_2$	Sigma-Aldrich
Polyvinylpyrrolidone (PVP)	C_3HO_6	Sigma-Aldrich
Propan-2-ol	$\text{C}_3\text{H}_8\text{O}$	CARLO ERBA
Maltodextrin	$\text{C}_{6n}\text{H}_{(10n+2)}\text{O}_{(5n+1)}$	Matsutani chemical industry Co.,Ltd.

3.2.1 Hydroxyapatite Powder

Hydroxyapatite Powder ($\text{Ca}_{10}(\text{PO}_4)_6(\text{OH})_2$) is the major component, and an essential ingredient, of normal bone and teeth. Hydroxyapatite used in this research has a particle size less than $2.5\mu\text{m} \pm 0.5 \mu\text{m}$ and has surface area larger than $100 \text{ m}^2/\text{g}$. The molecular weight of hydroxyapatite is 502.31 g/mol (Sigma-Aldrich Co.LLC).

3.2.2 Polyvinylpyrrolidone (PVP)

Polyvinylpyrrolidone (PVP) has a chemical formula $(\text{C}_6\text{H}_9\text{NO})_n$. PVP, also commonly called polyvidone or povidone, is a water soluble polymer made from the monomer N-vinylpyrrolidone. It is used as a binder. Polyvinylpyrrolidone is soluble in water and other polar solvent. For example, it is soluble in various alcohols, such as methanol and ethanol (Sigma-Aldrich Co.LLC).

3.2.3 Propan-2-ol (C₃H₈O)

Propan-2-ol or 2-propanol has the chemical formula C₃H₈ and structural formula CH₃CHOHCH₃. The molecular weight of 2-propanol is 60 g/mol (CARLO ERBA Reagents S.A.S).

3.2.4 Maltodextrin

Maltodextrin is produced from the starch by partial hydrolysis. Maltodextrin is easily digestible, being absorbed as rapidly as glucose and almost flavorless. Maltodextrin has the chemical formula C_{6n}H_(10n+1)O_(5n+1) and can disperse in water but is slightly soluble in anhydrous alcohol. (Matsutani chemical industry Co.,Ltd.)

3.3 Characterization of raw material (Hydroxyapatite powder, sodium chloride particles)

3.3.1 Phase analysis by means of X-ray diffraction (XRD)

3.3.2 Particles size distribution by means of laser diffraction analysis

(PSD) 3.3.3 Particles morphology by means of scanning electron microscope (SEM)

3.4 Preparation of hydroxyapatite slurry for spray drying

3.4.1 The hydroxyapatite slurry for spray drying was prepared following the procedure outline below. Preparation of hydroxyapatite slurry by mixing hydroxyapatite powder with maltodextrin as a binder and water as a solvent and

maltodextrin as a solid content 30% wt. and DARVAN C 1% wt. as a dispersing agent (Suwanprateeb et al., 2010). 3.4.2 Mixing slurry by magnetic stirrer and milling by ball mill for 6 hrs. The solid content of hydroxyapatite and maltodextrin in the slurry was kept 30% wt.

3.5 Spray drying condition

3.5.1 Spray drying of hydroxyapatite slurry at various drying conditions using (mini spray dryer, BUCHI B290), as shown in Table 3.4.

(a) Inlet drying air temperature

The experiments were carried out with various inlet drying air temperature such as 170°C is the temperature for liquid inside droplet evaporate and agglomerate, 200°C is intermediate temperature and 220°C is the maximum temperature of spray dryer.

(b) Drying air flow rate

Drying air flow rate was used at 35 m³/h that is maximum flow rate. However, at drying air flow rate 32 m³/h and 28 m³/h is actual flow rate can be used.

Figure 3.5 Aspirator settings versus throughput

(c) Slurry feed rate

Slurry feed rate or pump rate various were used 5, 10, 15 and 20 ml/min. The slurry feed rate at 5 ml/min is minimum feed rate that could be pumped the liquid into system and the spray drying could be working continuously. However, the slurry feed rate 20 ml/min is the maximum feed rate that can be spray droplet into system and evaporated to obtained agglomerate.

(d) Spraying air flow rate

The spraying air flow rate is the correlation between indicated height and volume throughput. The parameter adjusted with actual height is 30, 40 and 50 mm or 357, 473 and 601 l/h, respectively.

Figure 3.6 Conversion tables for spray drying parameters

Table 3.4 Experimental spray drying conditions.

No.	Inlet drying air temperature, °C	Drying air flow rate, m ³ /h	Slurry feed rate, ml/min	Spraying air flow rate, l/h
1	220	35	5	357
2	220	35	10	357
3	220	35	15	357
4	220	35	15	473
5	220	35	15	601
6	200	35	15	357
7	220	35	20	357
8	220	32	15	357
9	220	28	15	357
10	170	35	15	357

3.6 Characterization of spray-dried granules

3.6.1 Particles size distribution by means of laser diffraction analysis, (PSD).

3.6.2 Particles Morphology by means of scanning electron microscopy (SEM).

3.6.3 Flowability by measurement tap and loose density.

3.6.4 Density by tap density .

3.7 Preparation of the scaffold samples

3.7.1 The scaffold samples were prepared using the following procedure: Mixing hydroxyapatite granules with sodium chloride (NaCl) particles of different sizes including 250 μm , 325 μm and 400 μm at various ratios of hydroxyapatite to sodium chloride such as 50 : 50, 60 : 40, 40 : 60 and 30 : 70 wt%.

3.7.2 Mixing Polyvinylpyrrolidone (PVP) in 2-propanol ($\text{C}_3\text{H}_8\text{O}$) at 3 wt% to prepare the binder solution.

3.7.3 Spray Polyvinylpyrrolidone (PVP) binder solution on the top of formed sample and poured powder mixture with binder in mold. The mixture are flow in plasticity behavior.

3.7.4 Aging formed sample after PVP binder precipitation by wrapping the samples with the plastic film and keeping the sample for 6 hr.

3.7.5 After aging the formed sample was cooled as ambient temperature and dried in an oven at temperature 60 $^{\circ}\text{C}$ for 12 hr.

3.8 Characterization of formed samples before sintering

3.8.1 Microstructure by scanning electron microscope (SEM)

3.9 Sintering

3.9.1 To obtain the sintered scaffold samples, the formed samples was sintered at 1300 °C for 1 hr. with heating rate of 5°C / min. The firing curve is directed to soak 1 hour at 1300°C.

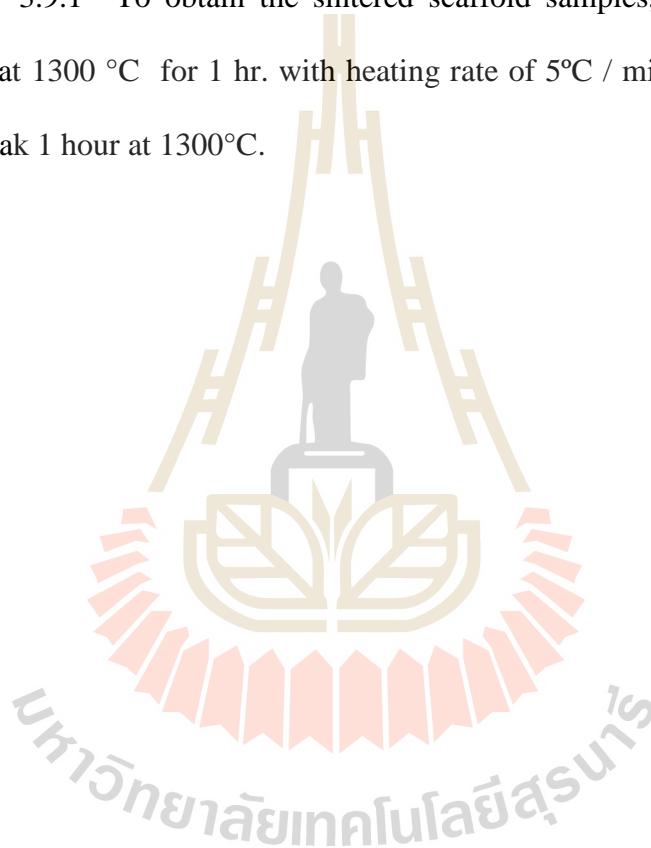


Figure 3.7 Diagram of sintering process of hydroxyapatite scaffolds.

3.10 Characterization of scaffold sample after sintering

3.10.1 Microstructure by scanning electron microscopy (SEM)

3.10.2 Interconnectivity by scanning electron microscopy (SEM)

3.10.3 Bulk density by Archimedes method

3.10.4 % True porosity by Archimedes method



Figure 3.8 Diagram of the first step : preparation of hydroxyapatite granules.

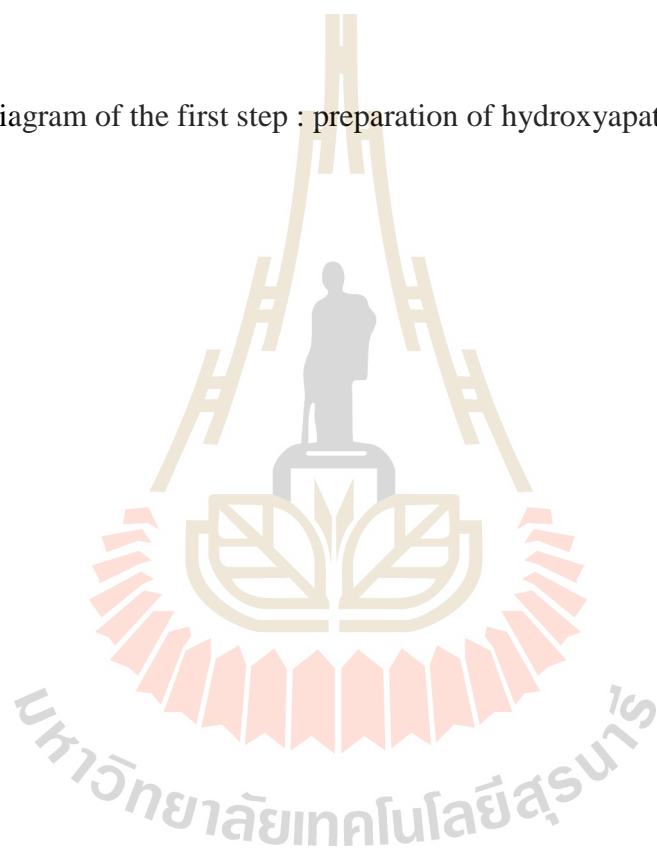
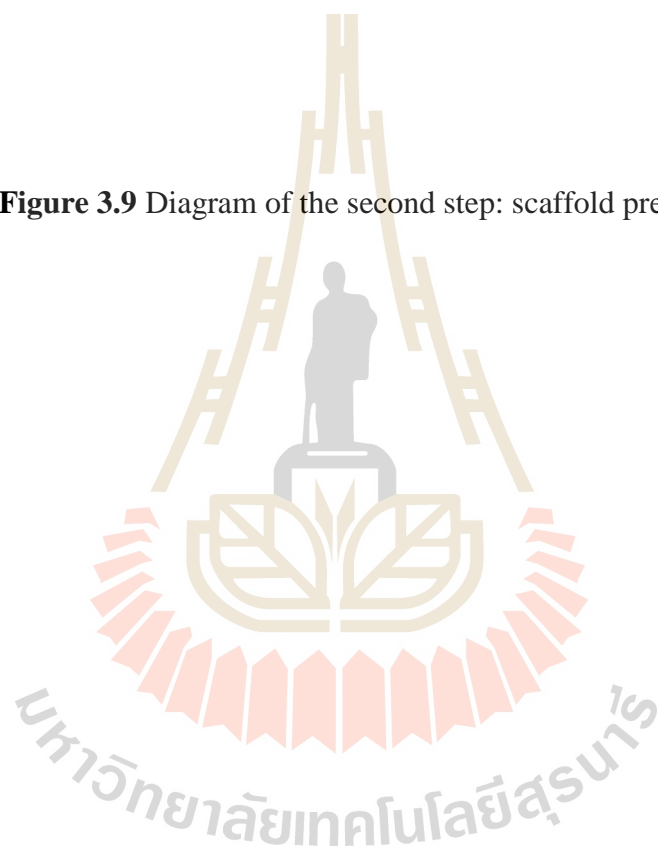


Figure 3.9 Diagram of the second step: scaffold preparation



CHAPTER IV

RESULT AND DISCUSSION

4.1 Hydroxyapatite raw material

4.1.1 Phase composition of hydroxyapatite raw material

Characterization phase hydroxyapatite powder by used X-ray diffraction (XRD) as show in fig 4.1 obtain to intensity maximum at 2θ is 31.80 and 32.0, respectively. Phase of raw material has only phase of hydroxyapatite (HA) is include a calcium and phosphate the mainly composition.

Figure 4.1 XRD pattern of hydroxyapatite as raw material powder

4.2 Effect of Process Parameters on Characteristics of Spray-dried Hydroxyapatite Granules

4.2.1 Morphology of hydroxyapatite granules at difference parameters

Figure 4.3 – 4.12 Result of characterization hydroxyapatite granule by scanning electron microscope (SEM) from figure show morphology of hydroxyapatite at magnification 800x in figure 4.3-4.12 (a) and magnification 3000x in figure 4.3-4.12 (b) the granule is show a good morphology has spherical shape and smooth surface.

However, hydroxyapatite granule at difference condition has a difference particle size and size distribution. The granule shape and morphology depend on spray drying conditions. The slurry composition and the rate of droplet evaporation are major factors that affect to granule shape and morphology. In this study, the slurry composition was kept constant. At high drying rate the dense particle layer is formed quickly at the droplet surface. Thus, the transport of water that evaporated in the granule to the outer granule surface is limited by the rate of diffusion of water vapor through the particle layer. As a result, the vapor pressure increases rapidly in the granule and the hole is formed by bursting the particle layer. The granules with the hole are observed at drying conditions at inlet drying air temperature 220 °C, drying air flow rate 35 m³/h, slurry feed rate 10 ml/min, spraying air flow rate 601 l/h, because the flow rate and temperature of drying air are high

enough to ensure the high drying rate of small size droplets generated at the high spraying air flow rate.

4.1.2 Effect of inlet drying air temperature

Inlet temperature is being the temperature of the heating drying air inside the chamber of spray drying. When spray drying a solution, the solvent is removed by vaporization. Increasing inlet drying air temperature results the evaporation efficiency and bulk density was decreased and effected to create hole inside particles and particles are broken while the droplet surface is evaporate quickly. However, the inlet drying air temperature 220°C is maximum temperature but it slightly effect to shape of hydroxyapatite granule as show in the Figure. 4.4, 4.8 and 4.11. Decreasing of inlet air temperature with condition no.3, 6 and 10, respectively the result shown smaller median particle size.

4.1.3 Effect of drying air flow rate

The median granule size was increased with decrease drying air flow rate as show with condition no. 3, 8 and 9. The drying air flow rate was adjusted to determine the actual volume flow for steady and repeat operating conditions it which is depending on the pressure drop of the overall system. Usually, a maximum air flow rate of approx. 35 m³/h.

4.1.4 Effect of slurry feed rate

The slurry feed rate or pump rate are relative feeding liquid into system for nozzle spray. The higher slurry feed rate was effected to by the reducing of outlet air temperature and increase the moisture content in the granule particles cause a lot of particle stick on the wall of spray dryer chamber. Moreover, the decreasing of slurry feed rate and spraying air flow rate in other word, the ratio of spraying air flow

rate and slurry feed rate higher ratio, the smaller granule particles and uniform size distribution were obtained. Therefore, two parameters are related to the median size and size distribution because the lower spraying air flow rate and feed rate will be affected to size of droplet spray dry.

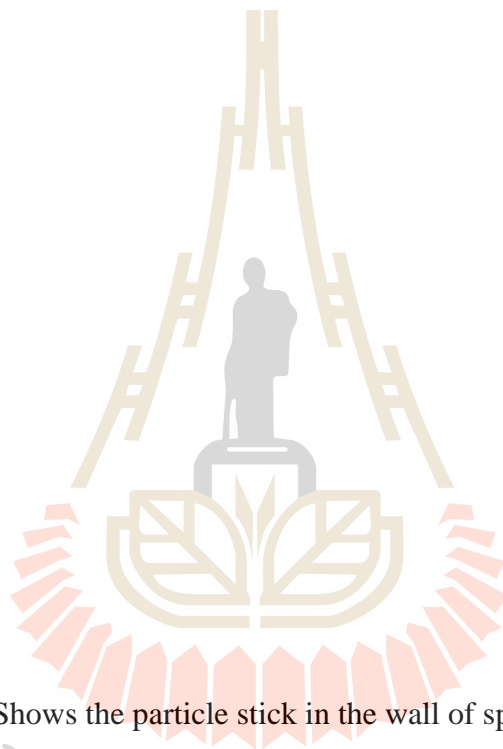


Figure 4.2 Shows the particle stick in the wall of spray drying chamber

4.1.5 Effect of spraying air flow rate

Generally, the high spraying air flow rate are increase with the pressure drop. With decreasing of spraying air flow rate, the granules particle are flow longer inside the spray dryer chamber—results lower moisture content due to higher evaporation rate. Thus, an increase of spraying air flow rate at constant slurry feed rate as the condition No. 3, 4 and 5, Table 3.4 results in a decreasing of granule median size and granule size distribution.

Figure 4.3 Scanning electron microscope of hydroxyapatite granule at inlet drying air temperature 220 °C, drying air flow rate 35 m³/h, slurry feed rate 5 ml/min, spraying air flow rate 357 l/h.

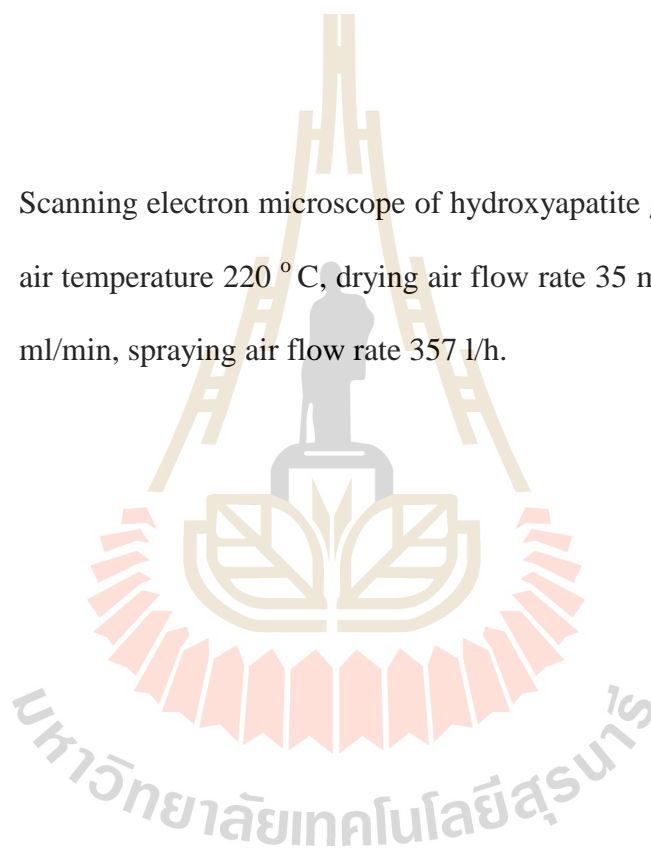


Figure 4.4 Scanning electron microscope of hydroxyapatite granule at inlet drying air temperature 220 °C, drying air flow rate 35 m³/h, slurry feed rate 15 ml/min, spraying air flow rate 357 l/h

Figure 4.5 Scanning electron microscope of hydroxyapatite granule at inlet drying air temperature 220 °C, drying air flow rate 35 m³/h, slurry feed rate 10 ml/min, spraying air flow rate 357 l/h

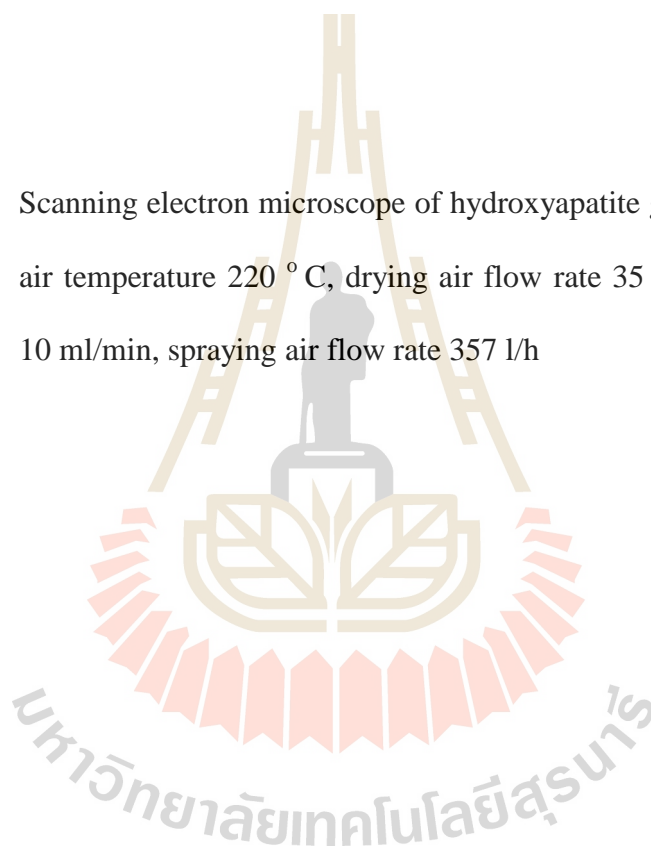


Figure 4.6 Scanning electron microscope of hydroxyapatite granule at inlet drying air temperature 220 °C, drying air flow rate 35 m³/h, slurry feed rate 10 ml/min, spraying air flow rate 473 l/h

Figure 4.7 Scanning electron microscope of hydroxyapatite granule at inlet drying air temperature 220 °C, drying air flow rate 35 m³/h, slurry feed rate 10 ml/min, spraying air flow rate 601 l/h

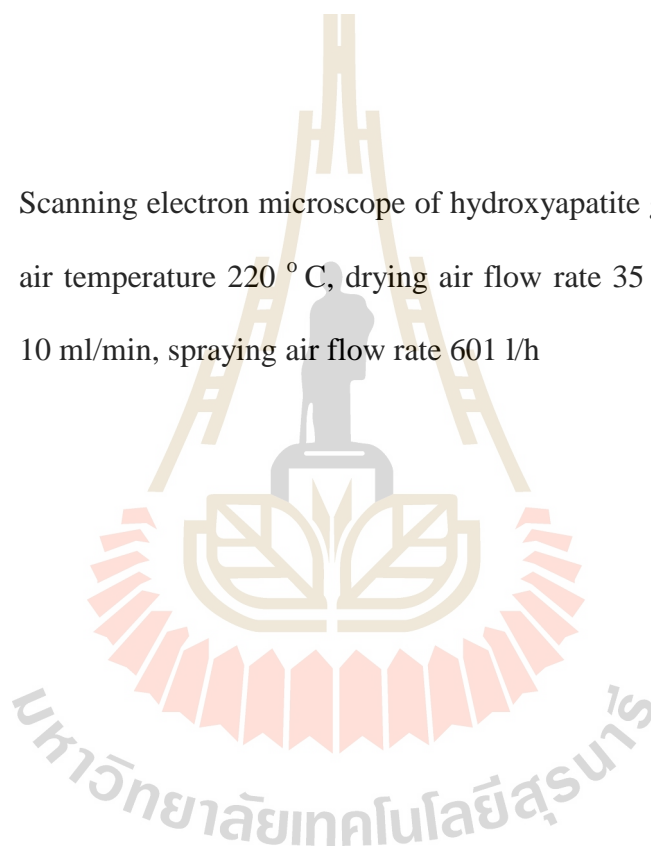


Figure 4.7 Scanning electron microscope of hydroxyapatite granule at inlet drying air temperature 200 °C, drying air flow rate 35 m³/h, slurry feed rate 15 ml/min, spraying air flow rate 357 l/h

Figure 4.9 Scanning electron microscope of hydroxyapatite granule at inlet drying air temperature 220 °C, drying air flow rate 35 m³/h, slurry feed rate 20 ml/min, spraying air flow rate 357 l/h

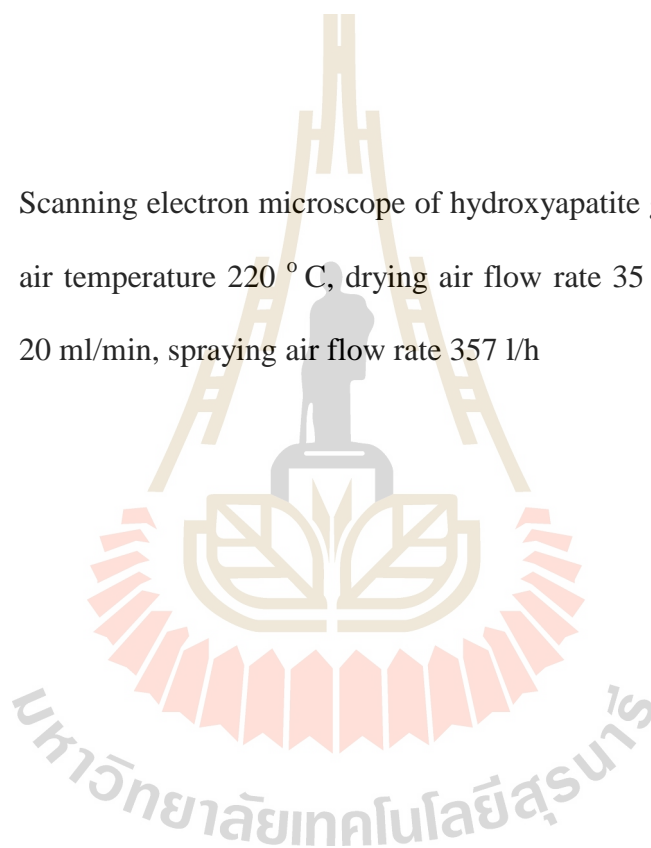


Figure 4. 10 Scanning electron microscope of hydroxyapatite granule at inlet drying air temperature 220 °C, drying air flow rate 32 m³/h, slurry feed rate 20 ml/min, spraying air flow rate 357 l/h

Figure 4.11 Scanning electron microscope of hydroxyapatite granule at inlet drying air temperature 220 °C, drying air flow rate 28 m³/h, slurry feed rate 20 ml/min, spraying air flow rate 357 l/h

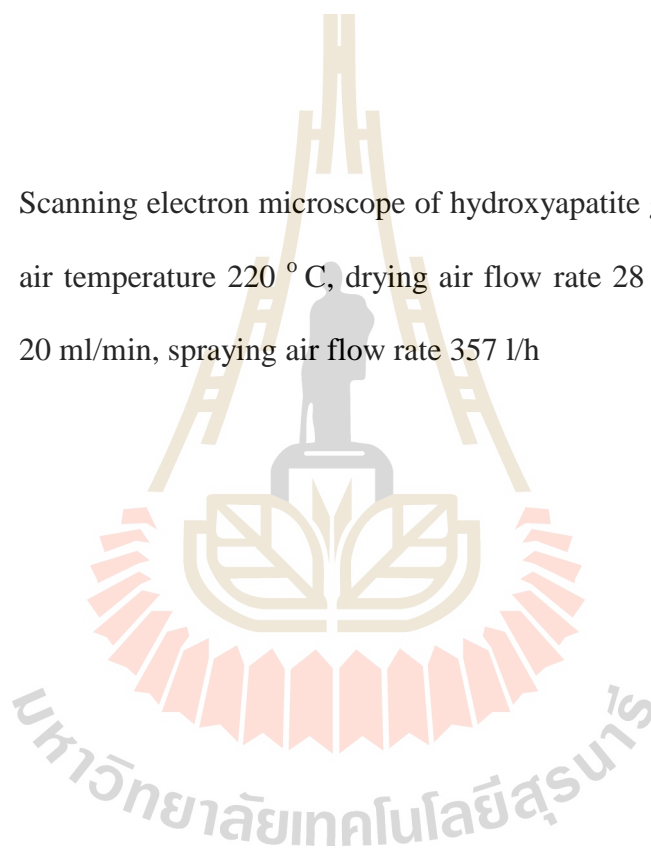


Figure 4.12 Scanning electron microscope of hydroxyapatite granule at inlet drying air temperature 170° C, drying air flow rate 35 m³/h, slurry feed rate 15 ml/min, spraying air flow rate 357 l/h

4.1.2 Particle size distribution of hydroxyapatite granules at difference parameters

Particle size distribution of hydroxyapatite granule from spray dryer depended the parameter of spray dry. Particle size distribution show the normal distribution with difference in median size (d_{50}) from 14.07 to 32.10 μm with narrow and uniform size distribution that are suitable for the scaffold structure. As the result, the narrower distribution and uniform granule size distribution were obtained with the condition No.5.

The ratio of spraying air flow rate to slurry feed rate effects to the median granule size and uniformity of granule size distribution. The higher the ratio, the smaller and more uniform spray-dried granules. The median granule size also increases with an increase in drying temperature (Run Nos. 10, 6, 3), and decrease in drying air flow rate (Run Nos. 3, 8, 9) and slurry feed rate (Run Nos. 7, 3, 2, 1).

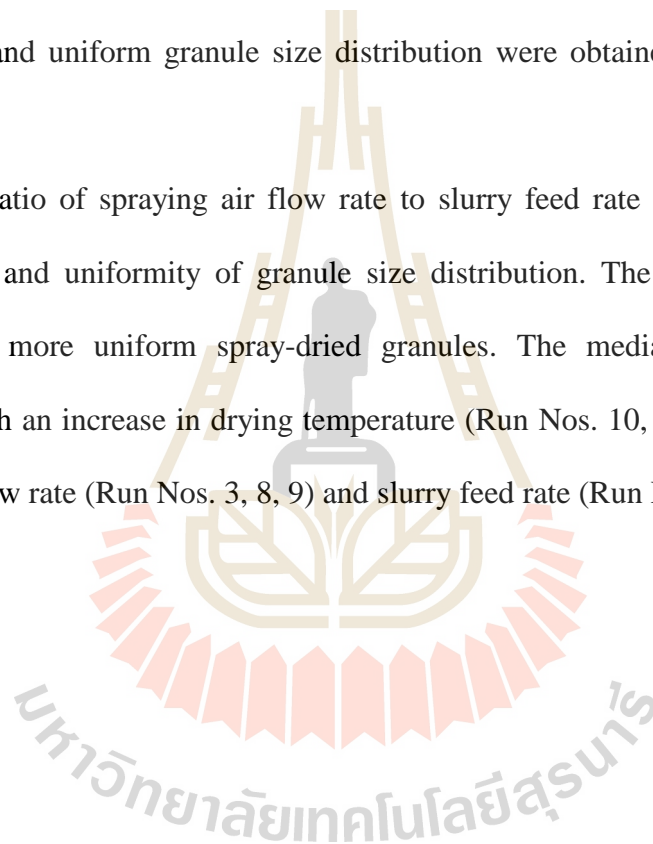


Figure 4.13 Show graph of particle size distribution of hydroxyapatite granule at inlet drying air temperature 220 °C, drying air flow rate 35 m³/h, slurry feed rate 5 ml/min, spraying air flow rate 357 l/h.

Figure 4.14 Show graph of particle size distribution of hydroxyapatite granule at inlet drying air temperature 220 °C, drying air flow rate 35 m³/h, slurry feed rate 15 ml/min, spraying air flow rate 357 l/h

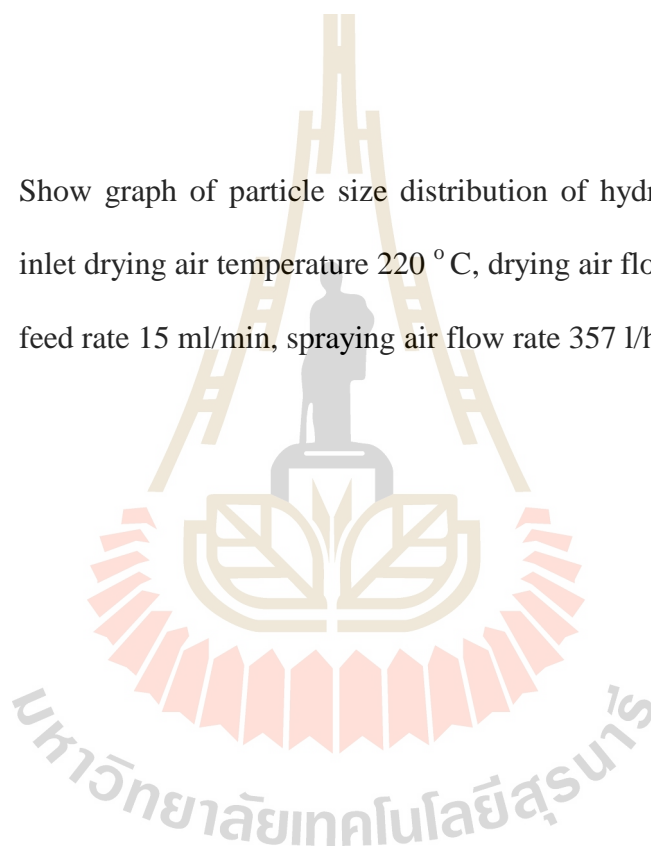


Figure 4.15 Show graph of particle size distribution of hydroxyapatite granule at inlet drying air temperature 220 °C, drying air flow rate 35 m³/h, slurry feed rate 10 ml/min, spraying air flow rate 357 l/h

Figure 4.16 Show graph of particle size distribution of hydroxyapatite granule at inlet drying air temperature 220 °C, drying air flow rate 35 m³/h, slurry feed rate 10 ml/min, spraying air flow rate 473 l/h

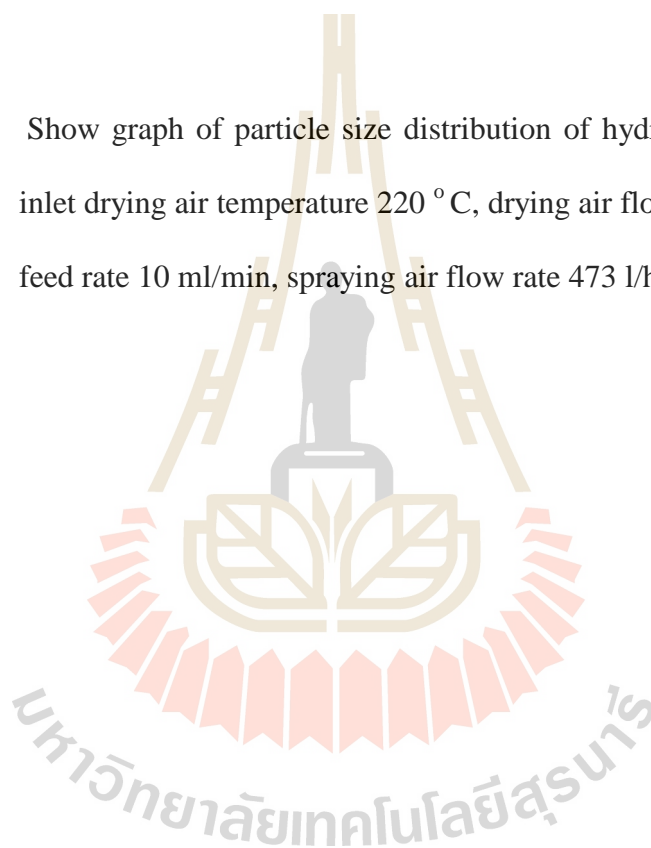


Figure 4.17 Show graph of particle size distribution of hydroxyapatite granule at inlet drying air temperature 220 °C, drying air flow rate 35 m³/h, slurry feed rate 10 ml/min, spraying air flow rate 601 l/h

Figure 4.18 Show graph of particle size distribution of hydroxyapatite granule at inlet drying air temperature 200 °C, drying air flow rate 35 m³/h, slurry feed rate 15 ml/min, spraying air flow rate 357 l/h

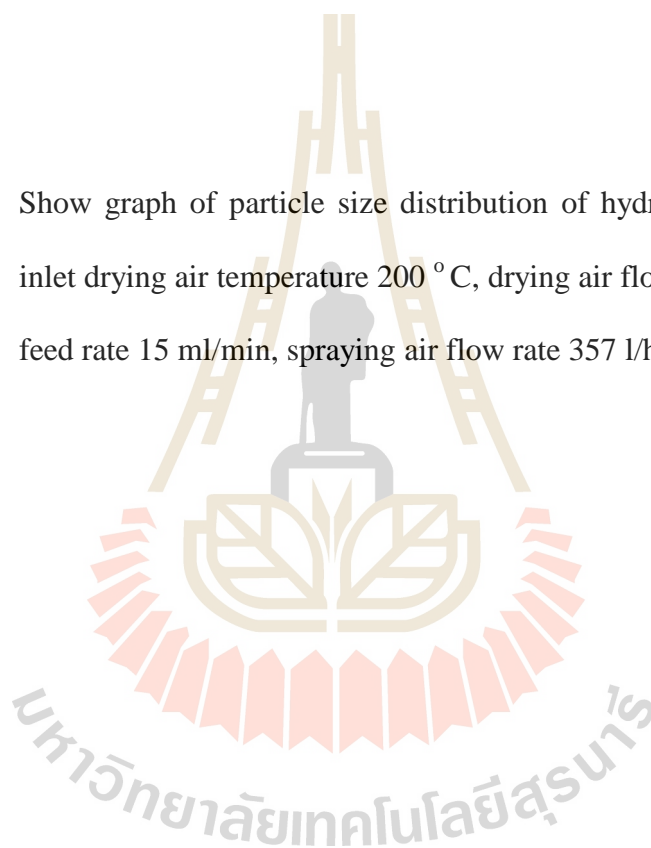


Figure 4.19 Show graph of particle size distribution of hydroxyapatite granule at inlet drying air temperature 220 °C, drying air flow rate 35 m³/h, slurry feed rate 20 ml/min, spraying air flow rate 357 l/h

Figure 4.20 Show graph of particle size distribution of hydroxyapatite granule at inlet drying air temperature 220 °C, drying air flow rate 32 m³/h, slurry feed rate 20 ml/min, spraying air flow rate 357 l/h

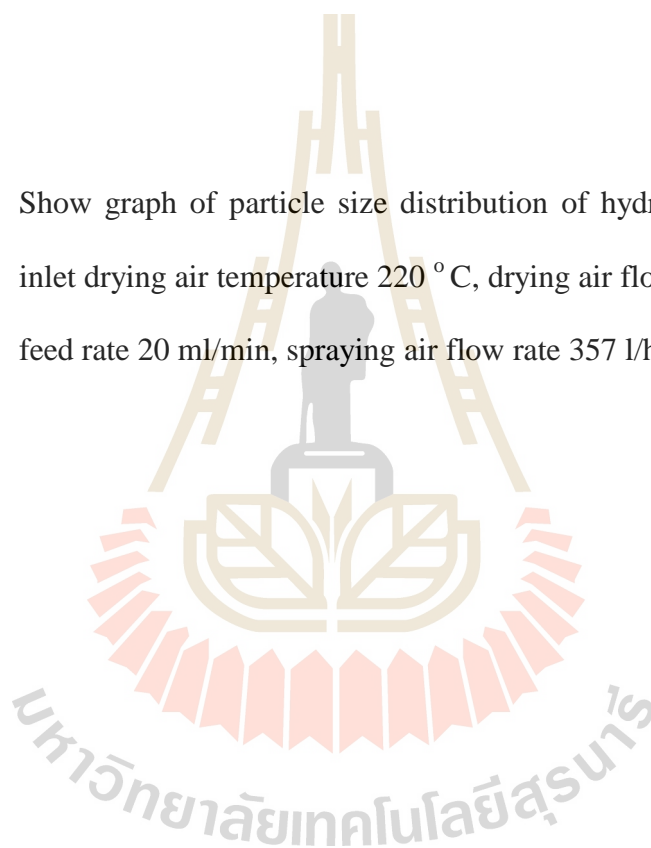


Figure 4.21 Show graph of particle size distribution of hydroxyapatite granule at inlet drying air temperature 220 °C, drying air flow rate 28 m³/h, slurry feed rate 20 ml/min, spraying air flow rate 357 l/h

Figure 4.22 Show graph of particle size distribution of hydroxyapatite granule at inlet drying air temperature 170°C , drying air flow rate $35\text{ m}^3/\text{h}$, slurry feed rate $15\text{ ml}/\text{min}$, spraying air flow rate $357\text{ l}/\text{h}$

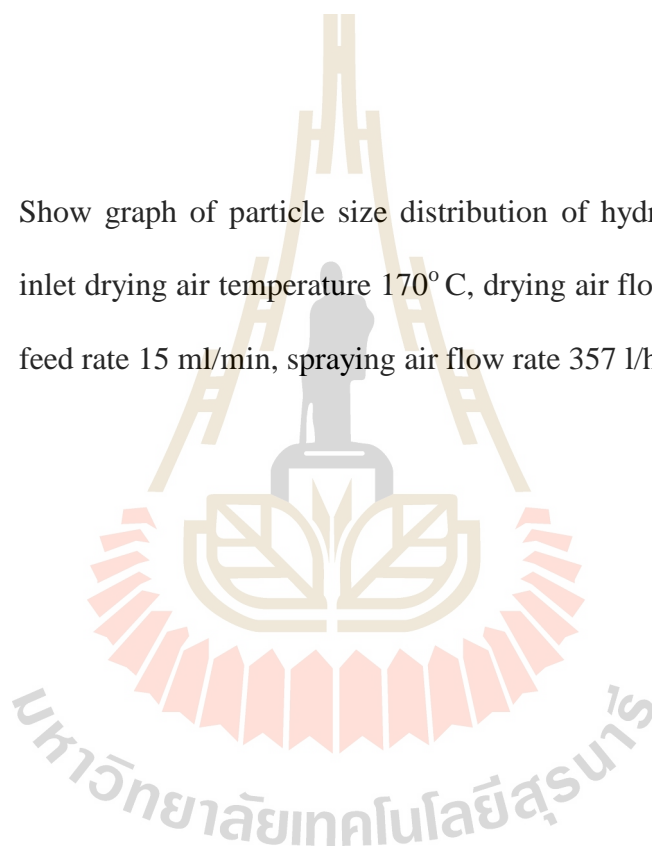


Table 4.1 Particle size distribution of hydroxyapatite granules prepared at different drying parameters.

Run No.	d ₁₀ (μm)	d ₅₀ (μm)	d ₉₀ (μm)	Span, (d ₉₀ -d ₁₀)/d ₅₀
1	16.01	31.60	57.71	1.320
2	13.96	29.39	52.63	1.316
3	8.93	19.73	51.08	2.136
4	7.45	16.57	42.81	2.134
5	8.75	16.50	32.12	1.416
6	10.06	20.08	40.24	1.503
7	7.87	17.91	43.67	1.999
8	13.57	30.47	56.37	1.405
9	14.28	32.10	65.15	1.585
10	7.02	14.07	35.21	2.004

4.1.3 Flow ability of hydroxyapatite granules at difference parameters

The flowability of spray-dried granules was evaluated by using the Hausner ratio and compressibility index. The Hausner ratio is defined as a ratio of the tapped density to the bulk density of powder by Eq. 1. Powder compressibility was estimated using Carr's compressibility index by Eq. 2. These indices could be determine the flowability of a granular material, as shown in Table 4.4

$$\text{Hausner ratio} = (\rho_T/\rho_B) \quad (4.1)$$

$$\text{Compressibility} = ((\rho_T - \rho_B)/\rho_T) \times 100 ,$$

(2) where ρ_B is the freely settled bulk density of the powder and ρ_T is the tapped bulk density of the powder.

Powder flowability depends on the particle size, shape and surface properties.

Large spherical particles with smooth non-cohesive surface often have good flow properties. The flowability can be correlated to the relative difference or the ratio of bulk and tapped densities. The tapped density of spray-dried granules varied from 0.55 to 0.95 g/ml and the bulk density from 0.30 to 0.49 g/ml depending on the process conditions, as summarized in Table 4.2.

Table 4.2 Bulk and tap densities of hydroxyapatite granules.

Run No.	Bulk density (g/ml)	Tap density (g/ml)	Run No.	Bulk density (g/ml)	Tap density (g/ml)
1	0.44	0.72	6	0.34	0.75
2	0.44	0.83	7	0.30	0.69
3	0.49	0.71	8	0.40	0.85
4	0.40	0.55	9	0.45	0.95
5	0.40	0.69	10	0.38	0.70

Table 4.3 Classification of hydroxyapatite granule flowability based on compressibility index and Hausner ratio.

Run No.	Compressibility index, %	Hausner ratio	Flowability
1	38.75	1.63	very, very poor
2	46.71	1.87	very, very poor
3	30.07	1.43	very poor
4	26.81	1.36	poor
5	41.23	1.70	very, very poor
6	53.88	2.16	very, very poor
7	56.12	2.27	very, very poor
8	52.31	2.09	very, very poor
9	52.18	2.09	very, very poor
10	45.15	1.82	very, very poor

The flowability of spray-dried granules was related to the tapped and bulk granule densities through the compressibility index and Hausner ratio (Table 4.3). The high values of compressibility index and Hausner ratio were observed at drying conditions Run Nos. 6 and 7 due to the small size and narrow size distribution of spray-dried granules. The compressibility index greater than 26 is considered to be an indication of poor powder flowability, and below 15 of good flowability according to Table 4.3. Our results confirm that the flowability of hydroxyapatite granules is classified as 'poor' or 'very poor' for every process conditions due to their relatively small sizes and cohesive surface properties as a result of using rather large amount of maltodextrin.

Table 4.4 Powder flowability and corresponding compressibility index and Hausner ratio

Compressibility index ,%	Powder flow characteristics	Hausner ratio
1-10	Excellent	1.00-1.11
12-15	Good	1.12-1.18
16-20	Fair	1.19-1.25
21-25	Passable	1.26-1.34
26-31	Poor	1.35-1.45
32-37	Very poor	1.46-1.59
> 38	Very, very poor	> 1.60

4.3 Characteristics of drying and sintering Hydroxyapatite scaffolds at various ratio and different size of Sodium chloride

4.3.1 Microstructure of hydroxyapatite scaffolds at various parameters before sintering

SEM pictures of hydroxyapatite scaffolds before sintering are show in the Figure 4.23 – 4.28 for different ratios of hydroxyapatite to sodium chloride and different sizes of sodium chloride. The microstructure of the scaffolds were analyzed by means of SEM at the same magnification. SEM images confirmed that, the sodium chloride and hydroxyapatite granules are not dissolved. Therefore, Polyvinypyrrolidone as a binder diluted in isopropanol does not dissolved the maltodextrin and sodium chloride. The formed hydroxyapatite scaffolds were strong

enough for handling as shown in Figure 4.23. The hydroxyapatite granule are dispersed between sodium chloride particles as shown in Figure 4.23-4.29. However, sodium chloride has higher weight more than hydroxyapatite granule which is effected on the uniform distribution of mixing. In order to avoid salt precipitation and segregation at the bottom of mold in the forming process, the experiment has been solved by increasing of mold size diameter to reduce the thickness of the formed samples.

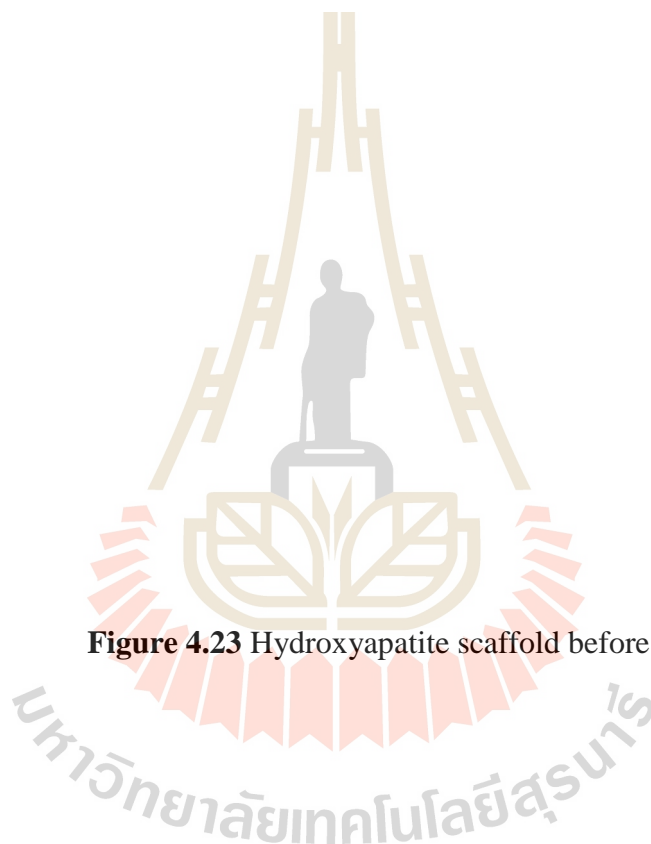


Figure 4.23 Hydroxyapatite scaffold before sintering

Figure 4.24 SEM image of hydroxyapatite scaffolds at hydroxyapatite to sodium chloride (NaCl) ratio 50: 50 using prepared of sodium chloride 250 μm .

Figure 4.25 SEM image of hydroxyapatite scaffolds at hydroxyapatite to sodium chloride (NaCl) ratio 50: 50 using prepared of sodium chloride 325 μm .

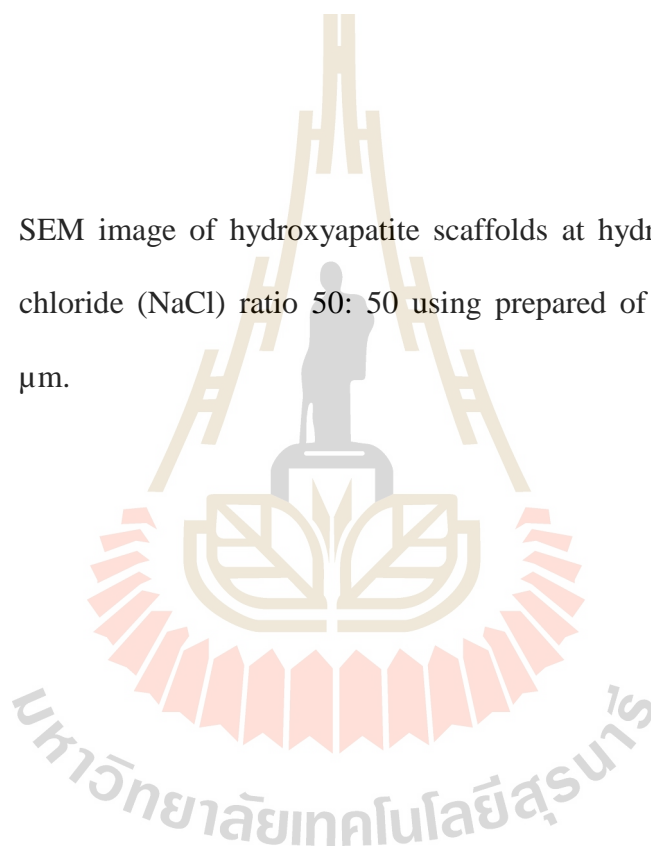


Figure 4.26 SEM image of hydroxyapatite scaffolds at hydroxyapatite to sodium chloride (NaCl) ratio 50 : 50 using prepared of sodium chloride 400 μm .

Figure 4.27 SEM image of hydroxyapatite scaffolds at hydroxyapatite to sodium chloride (NaCl) ratio 60 : 40 using prepared of sodium chloride 250 μm .

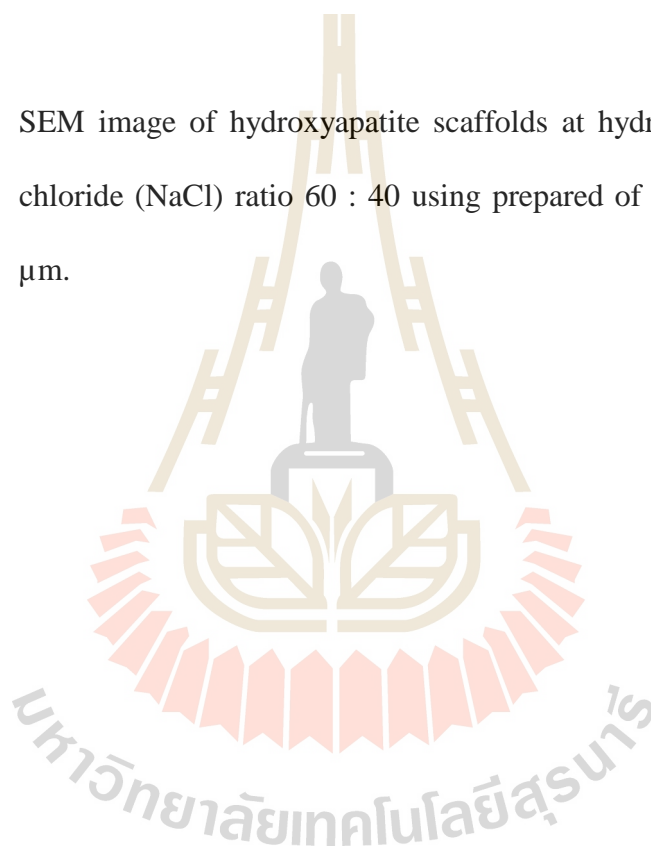


Figure 4.28 SEM image of hydroxyapatite scaffolds at hydroxyapatite to sodium chloride (NaCl) ratio 60 : 40 using prepared of sodium chloride 325 μm .

Figure 4.29 SEM image of hydroxyapatite scaffolds at hydroxyapatite to sodium chloride (NaCl) ratio 60 : 40 using prepared of sodium chloride 400 μm .

4.3.2 Microstructure sintered of hydroxyapatite

Figures 4.31-4.42 illustrates the microstructure of hydroxyapatite scaffolds prepared at different parameters and sintered at 1300°C. The scaffold after sintering show a lot of pores. The pores are formed inside hydroxyapatite granules and between granules. The hydroxyapatite scaffolds have pore sizes of 0.4 – 30 μm . The most of porosity cases from granules. After sintering, sodium chloride was completely burn out and confirmed by XRD pattern and Energy-dispersive x-ray analysis. However, the porosity and pore size of hydroxyapatite scaffold are favorably for cell growth. Pore size less than 1 μm are used for protein interaction and they are responsible for bioactivity. Pores of size between 1-20 μm are utilized for cell attachment.

Figure 4.30 Hydroxyapatite scaffold after sintered at 1300 °C for 1 hr.

The porosity after sintered at 1300 °C were obtained with the various as follows; I) The pores inside the hydroxyapatite granule preparation from spray dried. The hydroxyapatite granule contains hydroxyapatite powder and maltodextrin as a binder. The maltodextrin has melting point at 240°C it is a polysaccharide produced from the acidic or enzymatic hydrolysis of starch. It is considered a polymer of D-glucose chains linked by glycosides $-(1-4)$ and $-(1-6)$ bonds, and is formed by linear (amylase) and branched (amylopectin) carbohydrates with different equivalents of dextrose (Zenaida et al.). After sintering maltodextrin will burn out and leave the small pores inside granule II) The pores between hydroxyapatite granules were produced from granule surface then connected after sintering and obtained the interconnected pores. Moreover, the void inside of hydroxyapatite scaffold was produced from Polyvinylpyrrolidone binder burn out. Polyvinylpyrrolidone binder is completely combustible in the sintering process and therefore not effected to the hydroxyapatite scaffold microstructure.

II) The pores structure—from the sodium chloride burn out after sintered. The sodium chloride was completely burn out—confirmed by X-ray diffraction and Energy Dispersive X-Ray Analysis (EDX). After investigated by Energy Dispersive X-Ray Analysis (EDX) results show contains only calcium and phosphate ratio as shown in table 4.5 and investigated by Energy Dispersive X-Ray Analysis (EDX) as shown in—Figure 4.29. Therefore, sodium chloride evaporates are completely after sintering at 1300 °C.

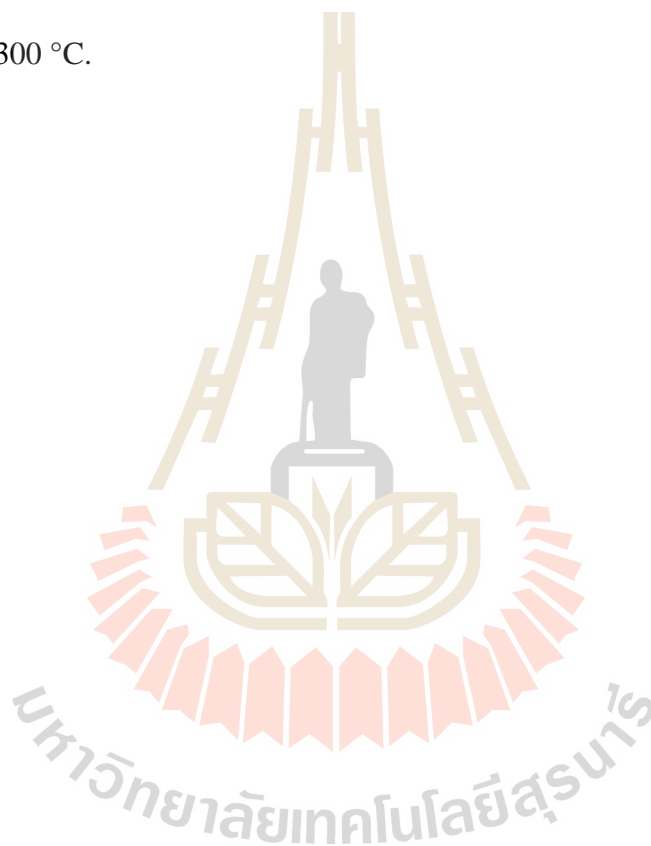


Figure 4.31 XRD pattern of hydroxyapatite after sintering at 1300°C

Figure 4.32 After sintered at 1300°C for 1 hr, the condition no.1 as show in. The hydroxyapatite granules shown a spherical shape and consist interconnection between granule particles. It showed the smaller pores inside granules particles. The porous between granules particles were occurred after burn out sodium chloride. The structure of scaffold after sintering in this condition seem strongly connected between granule particles.

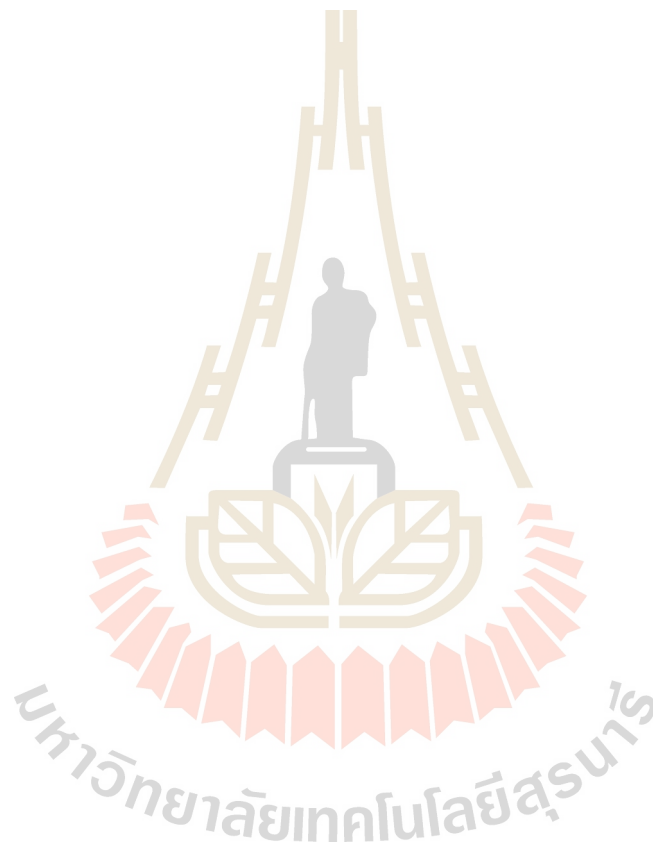


Figure 4.32 SEM photo of sintered hydroxyapatite scaffolds formed by mixing sodium chloride particle of 250 μm with spray dried hydroxyapatite granules at mixing ratio 50:50

After sintered at 1300°C the condition no.2 as show in Figure 4.33 The hydroxyapatite after sintered are not spherical shape. It showed connected particles, large pores after sodium chloride burn out and a lot of smaller pores between particles. Deformation of granules shape can occur from the forming process.

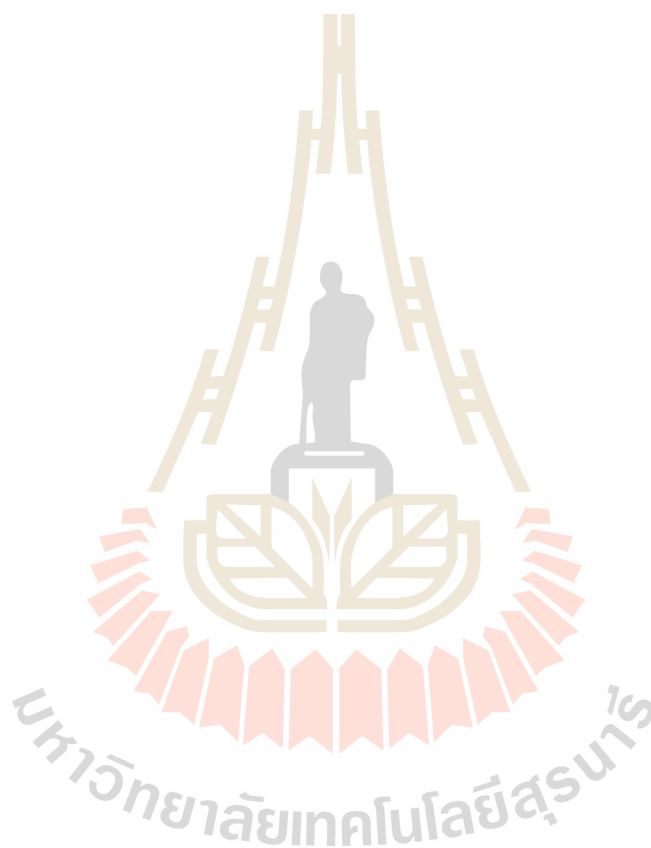


Figure 4.33 SEM photo of sintered hydroxyapatite scaffolds formed by mixing sodium chloride particle of 325 μm with spray dried hydroxyapatite granules at mixing ratio 50:50

Figure 4.34 After sintered at 1300°C for 1 hr, the condition no.3 as show in. The hydroxyapatite granules shown a spherical shape and consist interconnection between granule particles. It showed the smaller pores inside granules particles. The porous pore between granules particles were occurred after burn out sodium chloride. The structure of scaffold after sintering in this condition seem strongly connected between granule particles.

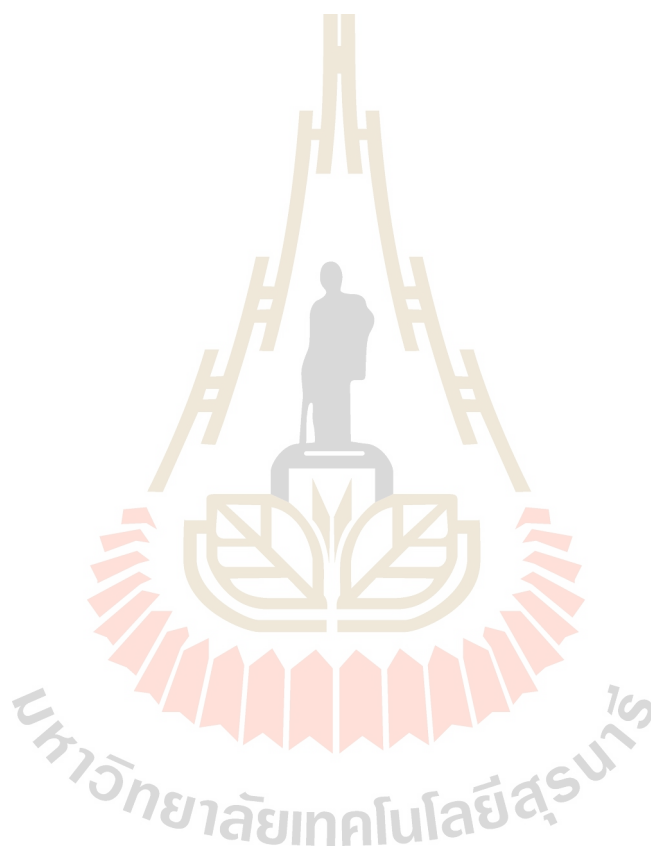


Figure 4.34 SEM photo of sintered hydroxyapatite scaffolds formed by mixing sodium chloride particle of 400 μm with spray dried hydroxyapatite granules at mixing ratio 50:50

Figure 4.35 After sintered at 1300°C for 1 hr, the condition no.4 as show in. The hydroxyapatite granules shown a spherical shape and consist interconnection between granule particles. It showed the smaller pores inside granules particles. The porous- between granules particles were occurred after burn out sodium chloride. The structure of scaffold after sintering in this condition seem strongly connected between granule particles.



Figure 4.35 SEM photo of sintered hydroxyapatite scaffolds formed by mixing sodium chloride particle of 250 μm with spray dried hydroxyapatite granules at mixing ratio 60:40

Figure 4.36 After sintered at 1300°C for 1 hr, the condition no.5 as show in. The hydroxyapatite granules shown a spherical shape and consist interconnection between granule particles. It showed the smaller pores inside granules particles. The porous between granules particles were occurred after burn out sodium chloride. The structure of scaffold after sintering in this condition seem strongly connected between granule particles.



Figure 4.36 SEM photo of sintered hydroxyapatite scaffolds formed by mixing sodium chloride particle of 325 μm with spray dried hydroxyapatite granules at mixing ratio 60:40

After sintered at 1300°C the condition no.6 as show in Figure 4.37 The surface of scaffold are not flat surface. In this condition the hydroxyapatite showed a lot of pores inside granules and still spherical shape. It showed pore between granules interconnected and large pores after sodium chloride burn out but the size of pore and porosity are different.



Figure 4.37 SEM photo of sintered hydroxyapatite scaffolds formed by mixing sodium chloride particle of 400 μm with spray dried hydroxyapatite granules at mixing ratio 60:40

Figure 4.38 After sintered at 1300°C for 1 hr, the condition no.7 as show in. The hydroxyapatite granules shown a spherical shape and consist interconnection between granule particles. It showed the smaller pores inside granules particles. The porous between granules particles were occurred after burn out sodium chloride. The structure of scaffold after sintering in this condition seem strongly connected between granule particles.

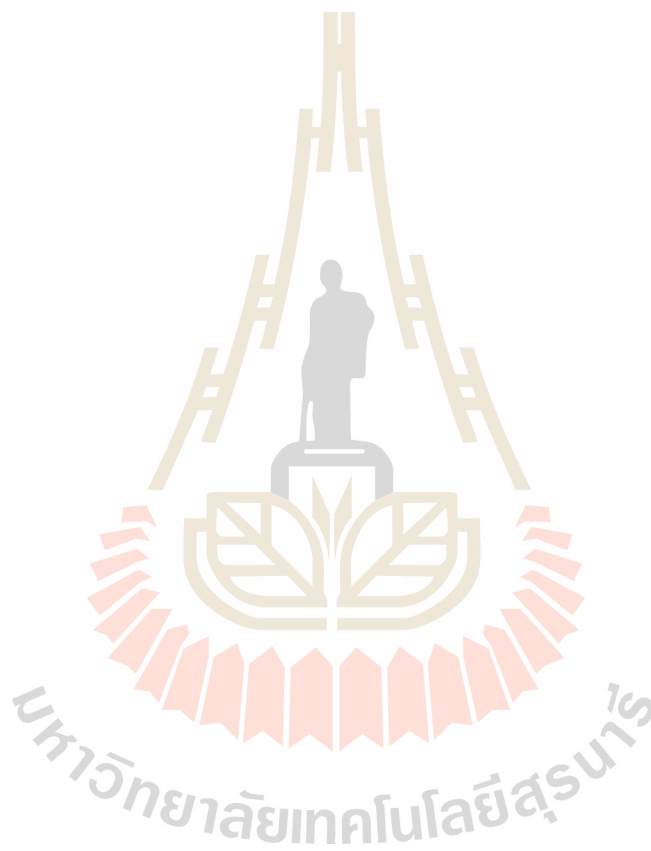


Figure 4.38 SEM photo of sintered hydroxyapatite scaffolds formed by mixing sodium chloride particle of 250 μm with spray dried hydroxyapatite granules at mixing ratio 40:60

After sintered at 1300°C the condition no.8 as show in Figure 4.39 The hydroxyapatite after sintered are not spherical shape. It showed connected particles, large pores after sodium chloride burn out and a lot of smaller pores between particles. Deformation of granules shape can occur from the forming process. However, the scaffold are present a lot of pores in the sample.

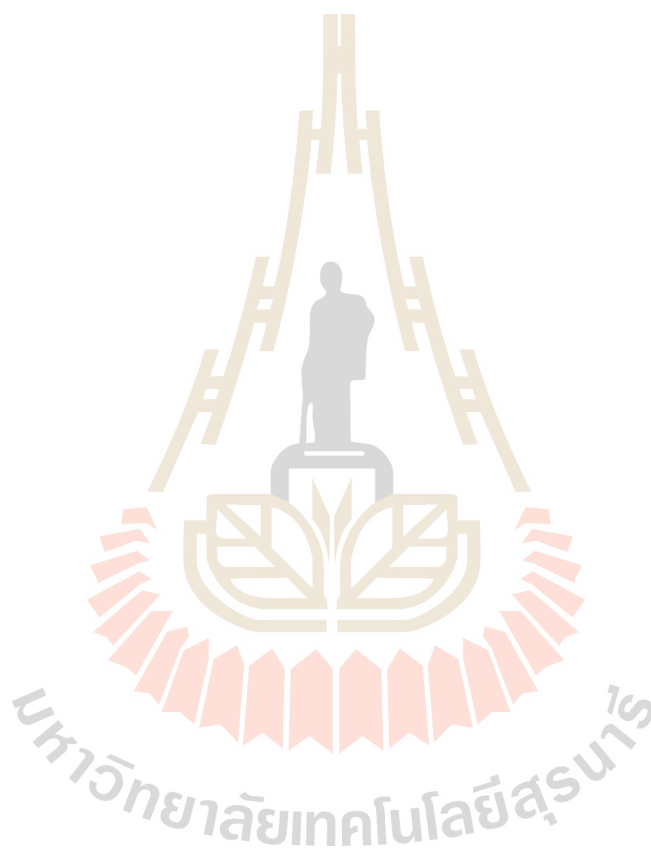


Figure 4.39 SEM photo of sintered hydroxyapatite scaffolds formed by mixing sodium chloride particle of 325 μm with spray dried hydroxyapatite granules at mixing ratio 60:40

Figure 4.40 After sintered at 1300°C for 1 hr, the condition no.9 as show in The hydroxyapatite granules shown a spherical shape and consist interconnection between granule particles. It showed the smaller pores inside granules particles. The porous between granules particles were occurred after burn out sodium chloride. The structure of scaffold after sintering in this condition seem strongly connected between granule particles.

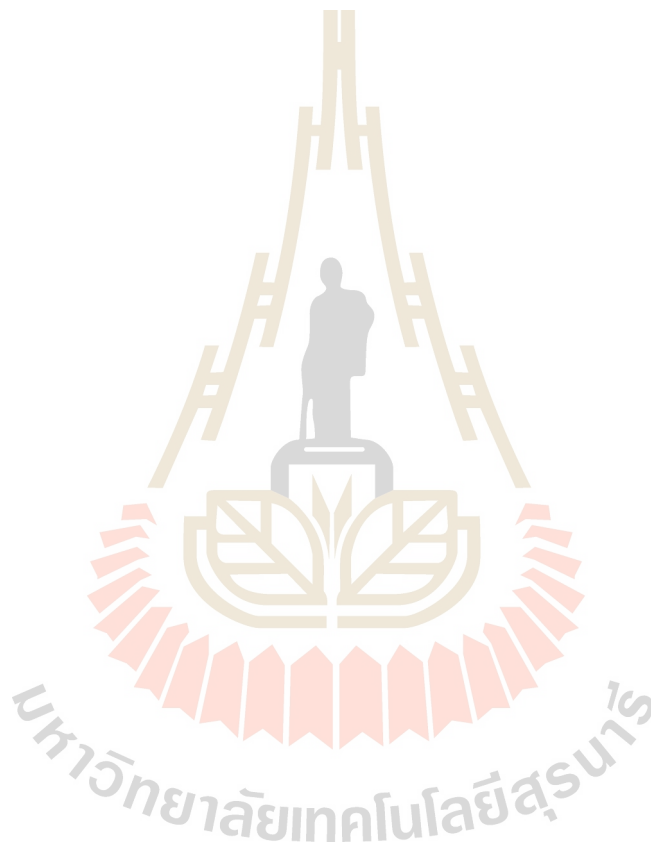


Figure 4.40 SEM photo of sintered hydroxyapatite scaffolds formed by mixing sodium chloride particle of 400 μm with spray dried hydroxyapatite granules at mixing ratio 60 : 40

After sintered at 1300°C the condition no.10 as show in Figure 4.41 The hydroxyapatite after sintered are not spherical shape. It showed connected particles, large pores after sodium chloride burn out and a lot of smaller pores between

particles. Deformation of granules shape can occur from the forming process. However, the scaffold are present a lot of pores in the sample.

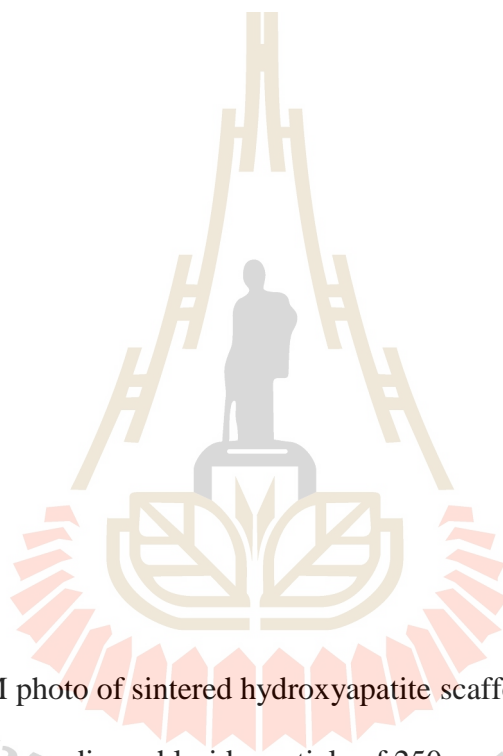


Figure 4.41 SEM photo of sintered hydroxyapatite scaffolds formed by mixing sodium chloride particle of 250 μm with spray dried hydroxyapatite granules at mixing ratio 30:70

After sintered at 1300°C the condition no.11 as show in Figure 4.42 The hydroxyapatite after sintered are not spherical shape. It showed connected particles, large pores after sodium chloride burn out and a lot of smaller pores between particles. Deformation of granules shape can occur from the forming process. However, the scaffold are present a lot of pores in the sample.

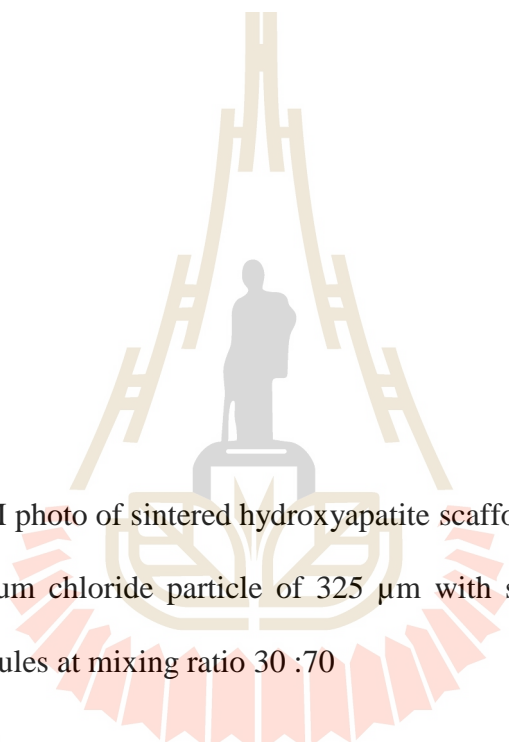
The image shows a scanning electron microscope (SEM) photograph of a sintered hydroxyapatite scaffold. The scaffold has a porous, interconnected structure. The pores are of various sizes, with some being significantly larger than others. The particles themselves are not perfectly spherical, indicating some deformation during the sintering process. The overall appearance is that of a highly porous, interconnected network of particles.

Figure 4.42 SEM photo of sintered hydroxyapatite scaffolds formed by mixing sodium chloride particle of 325 μm with spray dried hydroxyapatite granules at mixing ratio 30 :70

After sintered at 1300°C the condition no.12 as show in Figure 4.43 The hydroxyapatite after sintered are not spherical shape. It showed connected particles, large pores after sodium chloride burn out and a lot of smaller pores between particles. Deformation of granules shape can occur from the forming process. However, the scaffold are present a lot of pores in the sample.

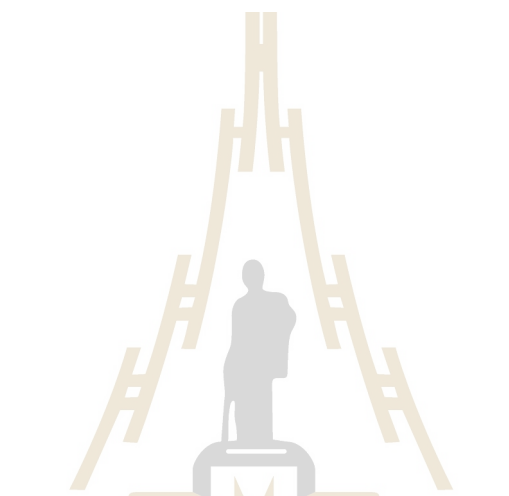
The image shows a scanning electron microscope (SEM) photograph of a sintered hydroxyapatite scaffold. The scaffold has a porous, interconnected structure with a central vertical channel. The structure is composed of multiple layers of interconnected struts, creating a lattice-like appearance. The struts are relatively uniform in thickness and are arranged in a way that allows for fluid flow through the central channel. The overall shape is roughly conical or cylindrical, tapering slightly towards the top. The background is dark, highlighting the metallic or ceramic texture of the scaffold.

Figure 4.43 SEM photo of sintered hydroxyapatite scaffolds formed by mixing sodium chloride particle of 400 μm with spray dried hydroxyapatite granules at mixing ratio 30:70

4.3.3 Characterization element composition of hydroxyapatite scaffolds

Table 4.5 Element composition of hydroxyapatite scaffold after sintering at 1300°C by using Energy-dispersive X-ray spectroscopy (EDX)

Sample Nos.	Ratio HA : NaCl	NaCl particle size (μm)	Calcium (Ca)		Phosphate (P)	
			Weight %	Atomic %	Weight %	Atomic %
1A	50 : 50	250	61.60	61.83	32.30	38.17
1B	50 : 50	325	71.74	66.24	28.26	33.76
1C	50 : 50	400	72.86	67.47	27.14	32.53
2A	60 : 40	250	71.06	65.49	28.94	34.51
2B	60 : 40	325	74.32	69.11	25.68	30.89
2C	60 : 40	400	73.22	67.88	26.78	32.12
3A	40 : 60	250	74.70	69.52	25.30	30.48
3B	40 : 60	325	68.24	62.41	31.76	37.59
3C	40 : 60	400	68.82	63.05	31.18	36.95
4A	30 : 70	250	-	-	-	-
4B	30 : 70	325	-	-	-	-
4C	30 : 70	400	-	-	-	-

4.3.4 True porosity and bulk density of hydroxyapatite scaffold

The bulk density and true porosity of scaffold are show in the table 4.6. The bulk density can calculate from mass per volume of scaffold after sintering and true porosity is obtained by Archimedes method. The Bulk density increases when the amount of HA increased and the true porosity increase when bulk density decrease.

The bulk density of sintered scaffold varies from 1.486 to 1.650 g/cm³ depending on HA : NaCl ratio and NaCl particle size. The true density varies from 52.63 to 68.83%, as summarized in Table 4.6.

Table 4.6 True porosity and bulk density of hydroxyapatite scaffold

Sample Nos.	Ratio	NaCl particle size (μm)	Bulk density (g/cm ³)	True porosity (%)
	HA : NaCl			
1A	50 : 50	250	1.582	55.42
1B	50 : 50	325	1.524	57.23
1C	50 : 50	400	1.507	58.21
2A	60 : 40	250	1.650	52.63
2B	60 : 40	325	1.581	56.14
2C	60 : 40	400	1.624	54.65
3A	40 : 60	250	1.500	58.00
3B	40 : 60	325	1.532	58.45
3C	40 : 60	400	1.497	60.07
4A	30 : 70	250	1.486	59.02
4B	30 : 70	325	1.495	64.47
4C	30 : 70	400	1.553	68.83

CHAPTER V

CONCLUSIONS

The preparation of hydroxyapatite with pores of different size was investigated in the present thesis. The scaffold were fabricated by mixing the agglomerate of fine hydroxyapatite particles prepared by spray drying with sodium chloride utilized as a porogen. The effect of spray dry conditions mixing ratio of sodium chloride to hydroxyapatite and size of sodium chloride particle were studies on the microstructure of hydroxyapatite scaffold sintered. The scaffold porous structure consists of interconnected micro pores in the agglomerate, meso pore in the agglomerate packing and macro pores formed after sodium chloride burn out.

The agglomerated fine of hydroxyapatite were collected in the size range of 7 to 65 μm depending on the drying conditions. The spray-dried granules with a void were obtained under drying conditions that support formation of small size droplets and their rapid drying. It was also found that the ratio of spraying air flow rate to slurry feed rate mostly effects to the uniformity of granule size distribution. The small granules were obtained at low drying air temperature, high drying air flow rate and high slurry feed rate. The high values of compressibility index and Hausner ratio corresponding to the low flowability were observed for spray-dried granules of small sizes and narrow size distributions.

The hydroxyapatite granules prepared by spray drying have a following characteristic:

1. Granule of spherical shape and smooth surface were prepared by spray drying at optimized condition.
2. The hydroxyapatite granule were of small, median and narrow size distribution. The hydroxyapatite scaffold was fabricated from hydroxyapatite run condition no.5 as it has a spherical shape and narrow distribution.
3. The flowability of hydroxyapatite granules was poor for every process conditions due to their relatively small sizes and cohesive surface properties as a result of using rather large amount of maltodextrin.
4. The granules have a small pore size inside the particle. The small pore size will obtained to various pore in scaffold it is a good properties.

The small pore were formed in the granule. These porous are important to fabricate cell growth in the scaffold. Sodium chloride as a porogen was used to generate large pore size in the scaffold. The scaffold fabrication process includes mixing of sodium chloride particles of various size with hydroxyapatite granules followed by sintering of powder mixture. At sintering temperature 1300 °C, 1 hr, sodium chloride was completely burns out and leaves large pore in the scaffold after sintering confirmed by X-ray diffraction and Energy Dispersive X-Ray Analysis (EDX) results shown only peak of hydroxyapatite and mainly element of hydroxyapatite include calcium and phosphate.

During sintering sodium chloride and PVA binder in the hydroxyapatite granule burned out completely and the scaffold with the complex porous structure was obtained including interconnected micro, meso and macro pores. The result of scaffold microstructure analysis can be summarize as follows:

1. The porous microstructure various with the size of sodium chloride particle difference size and hydroxyapatite: sodium chloride ratio. The hydroxyapatite scaffold have pore of various sizes between 0.4 – 30 μm . The pore size from 5-20 micrometers are proper for osteocytes cell attachment and proliferation penetration. The osteocytes cell is type of bone cell is most commonly found cell in bone tissue.

2. The pores in the hydroxyapatite granule and between granules were interconnected pores. In summary, the spray drying of hydroxyapatite slurry was successfully accomplished and granules of round shape with smooth surface. The hydroxyapatite scaffolds manufactured using hydroxyapatite granule and sodium chloride as a porogen possessed the porous structure with various size pore. The porosity of scaffold was controlled by the amount of sodium chloride added. The strength and body compatibility of scaffold should be tested in future research.

REFERENCES

- T. Garima, B. Bikramjit. (2012). A porous hydroxyapatite scaffold for bone tissue engineering: Physic mechanical and biological evaluations. *Ceramics International*, Vol.38, Issue 1(P. 341-349).
- U. Mayo, O. Masahiro, T. Shoji, M. Naoyuki. (2013). Preparation and characterization of lowcrystallized hydroxyapatite nanoporous plates and granules. *Applied Surface Science*, Vol.287 (P.195-202).
- A.E. Pepla, L.K. Besharat, G.Palaia, G.Tenore, G.Migliau. (2014). Nano-hydroxyapatite and its applications in preventive, restorative and regenerative dentistry: a review of literature. DOI: 10.11138/ads/2014.5.3.108
- L. Wang, L. Wang, Ch.Wang, J. Qin, Z. Wu, S. Song. (2015). Effect of preparation process on tensile strength of nano-hydroxyapatite/polyetheretherketone composite materials. DOI: 10.1109/TENCON.2015.7373112.
- S. Keshani, W.R.W. Daud, M.M. Nourouzi, F. Namvar, M. Ghasemi. (2015). Spray drying: an overview on wall deposition. *Journal of Food Engineering, process and modeling*, Vol.146 (P.152-162).

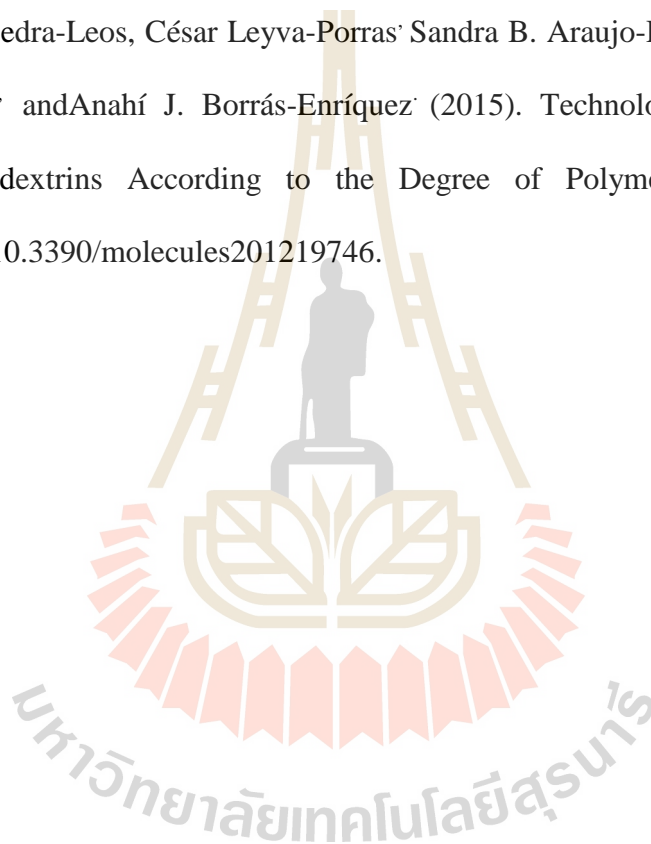
- J. Suwanprateeb, R. Sanngam, T. Panyathanmaporn. (2010). Influence of raw powder preparation routes on properties of hydroxyapatite fabricated by 3D printing technique. *Material Science Engineer*, Vol.30, Issue 4 (P.610-617).
- W. Julklang, B.Golman. (2015). Numerical simulation of spray drying of hydroxyapatite nanoparticles, *Clean Technologies and Environmental Policy*, Vol. 17, Issue 5 (P.1217–1226)
- C. Gholamreza, T. Mojtaba. (2013). Whey powder: process technology and physical properties: A review, *Middle-East Journal of Scientific Research*, 10, 1377-1387. DOI: 10.5829/idosi.mejsr.2013.13.10.1239.
- Richard E. Rimana, Wojciech L. Suchaneka, Kullaiiah Byrappa, Chun-Wei Chen, Pavel Shuka, Charles S. Oakesa. (2002). Solution synthesis of hydroxyapatite designer particulates, *Solid State Ionics*. Volume 151, Issues 1–4 (P.393–402).
- Yoon Sung Nam, Jun Jin Yoon, Tae Gwan Park. (2000). A Novel Fabrication Method of Macroporous Biodegradable Polymer Scaffolds Using Gas Foaming Salt as a Porogen Additive. Department of Biological Sciences, Korea Advanced Institute of Science and Technology, Taejon 305-701, Volume 53, Issue 1 (P.1–7), South Korea.
- Paul Tomlins, Paul Grant, Sergey Mikhalovsky, Stuart James, and Lyuba Mikhalovska. (2004). Measurement of pore size and porosity of tissue scaffolds, *Journal of ASTM International*, Jan. 04, Vol. 1, No.1 (P.1-8).

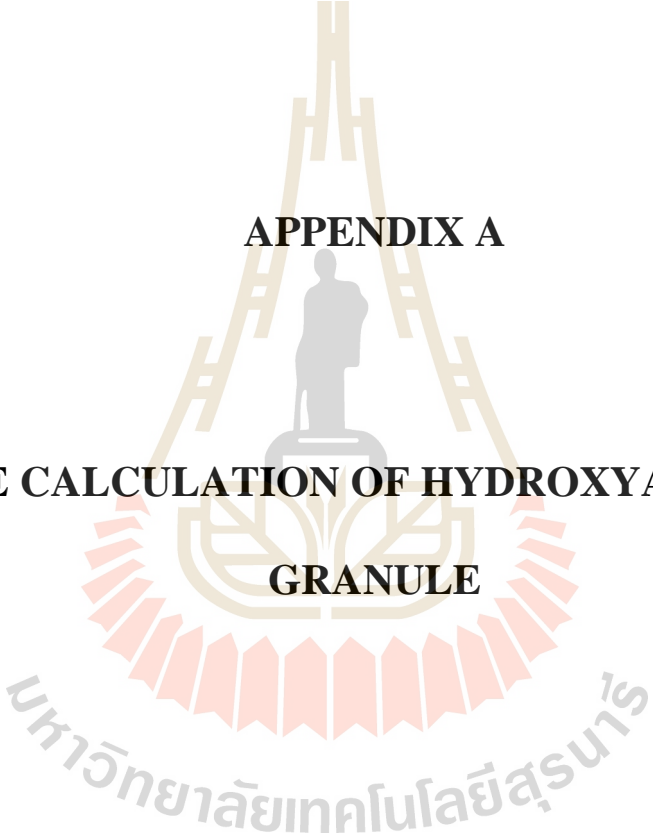
- V.P.Orlovskill, V.S.Komlev and S.M.Barinov. (2002). Hydroxyapatite and hydroxyapatite- based ceramics. *Inorganic materials*, Volume 38, Issue 10 (P.973–984)
- Hassna Rehnam Ramay, Miqin Zhang. (2003). Preparation of porous hydroxyapatite scaffolds by combination of the gel-casting and polymer sponge methods. *Biomaterials*, Volume 24, Issue 19 (P.3293-3302)
- Susmita Bose, Mangal Roy, and Amit Bandyopadhyay. (2012). Recent advances in bone tissue engineering scaffolds. *Trends in Biotechnology*, October, Vol.30, No.10 (P.546-554)
- Mehdi Kazemzadeh Narbat, Faruba Orang, Mehran Solati Hashtjin and Azadeh Goudarzi. (2016). Fabrication of porous Hydroxyapatite-Gelatin composite scaffolds for bone tissues engineering. *Iranian Biomedical Journal*. Volume 4, Issue 1 (P. 54-60).
- Yuzhang Du, Xiaofeng Chen, Young Hag Koh, Bo Lei. (2014). Facilely fabrication PCL nanofibrous scaffolds with hierarchical pore structure for tissue engineering. *Vol.122* (p.62-65).
- Sanosh Kunjalukkal Padmanabhan, Francesca, Gervaso, Alessandro Sannino, and Antonio Licciulli. (2014). Preparation and characterization of collagen/hydroxyapatite microsphere composite scaffold for bone regeneration. *Key Engineering Materials* Vol.587 (p.239-244)
- Richard T. Tram, Elhum Naseri, Aleksey Kolasnikov, Xiaochun Bai and Jian Yang. (2011). A new generation of sodium chloride porogen for tissue engineering.

Biotechnology and Applied Biochemistry, Volume58, Issue 5
September/October (P.335–344)

Bich T. N. Phan, Hanh T. Nguyen¹, Huong Q. Dao, Lam V. Pham, Trang T. T. Quan, Duong B. Nguyen, Huong T. L. Nguyen, Thuan T. Vu. (2017).
Materials Science and Engineering. Vol.30, Issue 4 (P.610-617).

Zenaida Saavedra-Leos, César Leyva-Porras¹ Sandra B. Araujo-Díaz, Alberto Toxqui-
Terán¹ and Anahí J. Borrás-Enríquez¹ (2015). Technological Application of
Maltodextrins According to the Degree of Polymerization. Molecules,
DOI:10.3390/molecules201219746.





APPENDIX A

**THE CALCULATION OF HYDROXYAPATITE
GRANULE**

I) The calculation of particle size distribution

This result from machine. It data show $D_{v0.1}$, $D_{v0.5}$, $D_{v0.9}$, median size, mean size, Stand deviation, graph distribution and table data in the excel program. Span is parameter to show the width of the size distribution. The span of a volume-based size distribution is defined as

$$\text{Span} = (D_{v0.9} - D_{v0.1}) / D_{v0.5}$$

(Eq.A1)

Example A1

Data from machine is

$$D_{v0.9} = 32.12 \mu\text{m}$$

$$D_{v0.5} = 16.50 \mu\text{m}$$

$$D_{v0.1} = 8.75 \mu\text{m}$$

From Eq.A1

$$\text{Span} = (32.12 - 8.75) / 16.50 = 1.416$$

Figure A1 Result from particle size distribution of hydroxyapatite granule.

II) The calculation of Hausner ratio and Compressibility of hydroxyapatite granule

$$\text{Hausner ratio} = (\rho_T/\rho_B) \quad (\text{Eq.A2})$$

where;

ρ_T = Tapped bulk density of powder

ρ_B = Bulk density of powder

Example A2 Data from experimental are following table4.2 Page 57

$$\rho_T = 0.72 \text{ g/ml}^3$$

$$\rho_B = 0.44 \text{ g/ml}^3$$

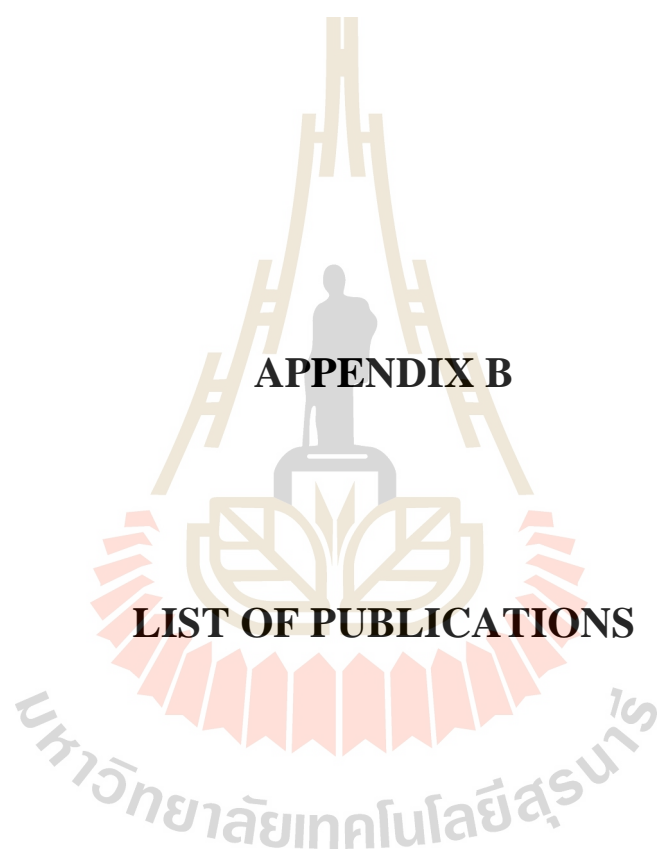
From Eq.A2 Hausner ratio = $(0.72/0.44) = 1.63$

$$\text{Compressibility} = ((\rho_T - \rho_B)/\rho_T) \times 100 \quad (\text{Eq.A3})$$

Example A3 Data from experimental are following table4.2 Page 57

From Eq.A3 Compressibility = $((0.72 - 0.44)/0.72) \times 100 =$
38.75%

มหาวิทยาลัยเทคโนโลยีสุรนารี



APPENDIX B

LIST OF PUBLICATIONS

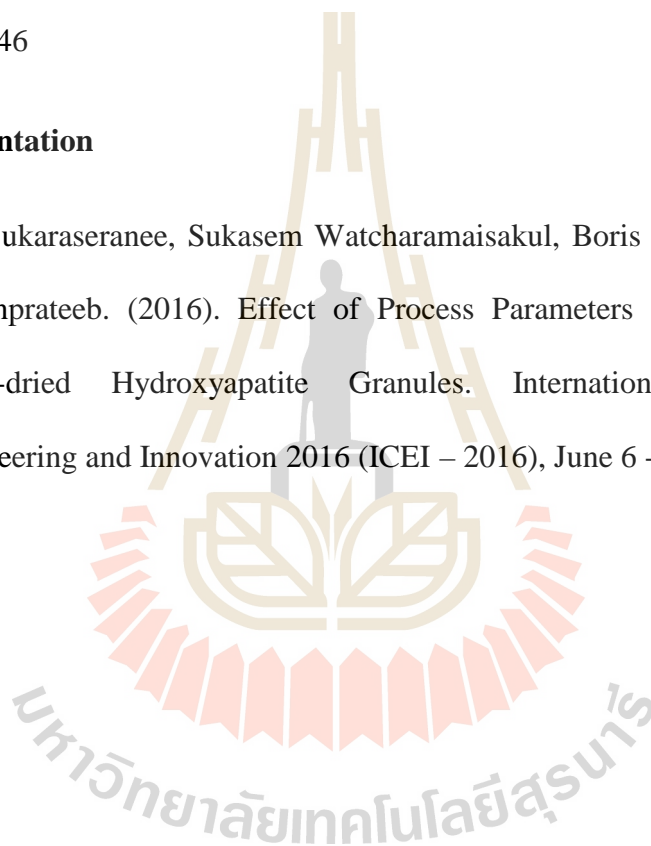
LIST OF PUBLICATIONS

I. Papers

Weeranuch Sukaraseranee, Sukasem Watcharamaisakul, Boris Golman and Jintamai Suwanprateeb. (2016). Effect of Process Parameters on Characteristics of Spray-dried Hydroxyapatite Granules. Key Engineering Materials Vol. 728, pp 341-346

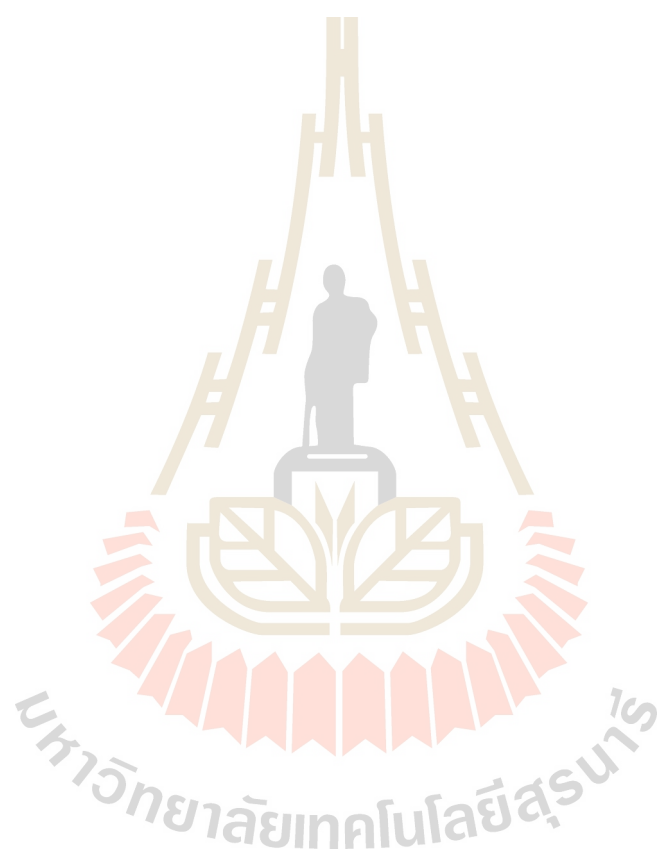
II. Presentation

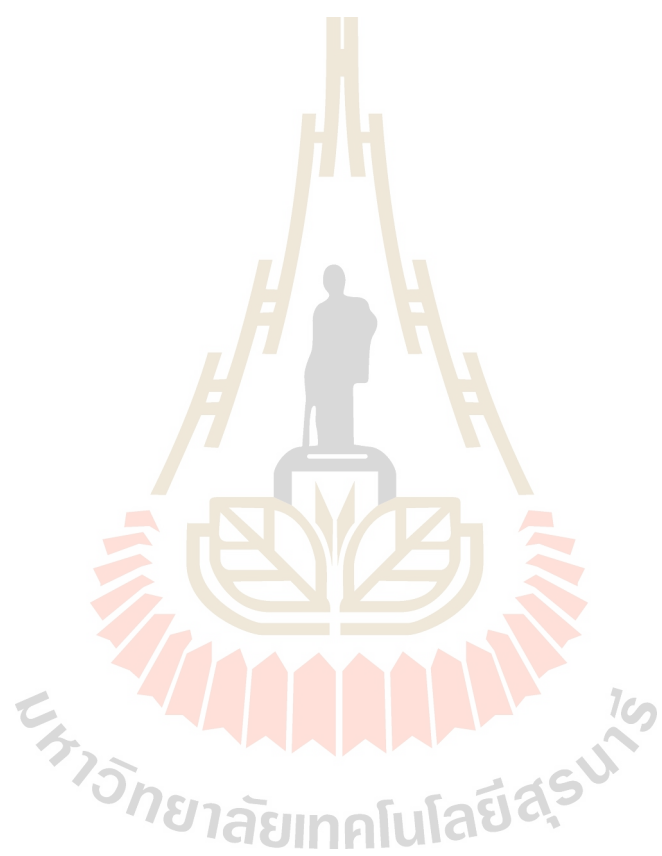
Weeranuch Sukaraseranee, Sukasem Watcharamaisakul, Boris Golman and Jintamai Suwanprateeb. (2016). Effect of Process Parameters on Characteristics of Spray-dried Hydroxyapatite Granules. International Conference on Engineering and Innovation 2016 (ICEI – 2016), June 6 - 7, 2016.



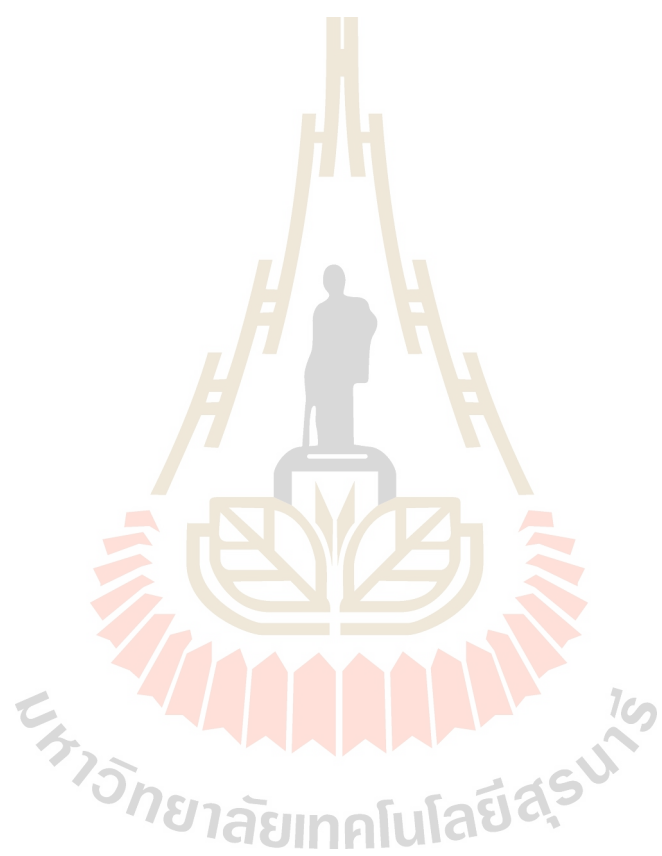












BIOGRAPHY

Weeranuch Sukaraseranee was born on January 25th, 1992 in Nakhonratchasima Province, Thailand. She graduated high school from Pakchong school in 2013 and graduated Bachelor Degree in Ceramic Engineering from Suranaree University of Technology in 2016. I received a scholarship OROG from Suranaree University of Technology for Master Degree in Ceramic Engineering. She is a teacher assistance of Ceramic laboratory, Suranaree University of Technology in 2016. In 2017, she work in quality control engineer at Thai-German Ceramic industry Public Company Limited (Thailand). In the present, She work in researcher at Noritake SCG Co., Ltd. During she study Master Degree, she has published a paper entitled “Effect of Process Parameters on Characteristics of Spray-dried Hydroxyapatite Granules” in Key Engineering Materials Vol. 728, pp 341-346